

Automated Computation of Autonomous Spectral Submanifolds for Nonlinear Modal Analysis

Sten Ponsioen^a, Tiemo Pedergnana^a, George Haller^{a,*}

^a*Institute for Mechanical Systems
ETH Zürich, Leonhardstrasse 21, 8092 Zürich, Switzerland*

Abstract

We discuss an automated computational methodology for computing two-dimensional spectral submanifolds (SSMs) in autonomous nonlinear mechanical systems of arbitrary degrees of freedom. In our algorithm, SSMs, the smoothest nonlinear continuations of modal subspaces of the linearized system, are constructed up to arbitrary orders of accuracy, using the parameterization method. An advantage of this approach is that the construction of the SSMs does not break down when the SSM folds over its underlying spectral subspace. A further advantage is an automated a posteriori error estimation feature that enables a systematic increase in the orders of the SSM computation until the required accuracy is reached. We find that the present algorithm provides a major speed-up, relative to numerical continuation methods, in the computation of backbone curves, especially in higher-dimensional problems. We illustrate the accuracy and speed of the automated SSM algorithm on lower- and higher-dimensional mechanical systems.

Keywords: spectral submanifolds, model order reduction, nonlinear normal modes, structural dynamics, backbone curves.

1. Introduction

A fundamental notion in decomposing nonlinear mechanical oscillations, is the *nonlinear normal mode* (NNM) concept of Rosenberg [1], who defined a nonlinear normal mode as a synchronous periodic oscillation that reaches its maximum in all modal coordinates at the same time. An alternative definition of a NNM, proposed by Shaw and Pierre [2], is an invariant manifold that serves as the nonlinear continuation of two-dimensional subspaces formed by normal modes of the linearized system. Shaw and Pierre seek such invariant manifolds as graphs over those two-dimensional subspaces. For several extensive discussions about these two NNM definitions, we refer the reader to the work of Kerschen et al. [3], Peeters et al. [4], Mikhlin and Avramov [5] and Vakakis et al. [6].

If one relaxes the synchronicity requirement of Rosenberg, a clear relationship between the above two views on NNMs emerges for conservative oscillatory systems by the Lyapunov subcenter-manifold theorem [7, 8]. Indeed, under appropriate non-resonance conditions, these references guarantee the existence of a unique, analytic and robust Shaw—Pierre-type invariant manifold tangent to each two-dimensional modal subspace of the linearized system. This manifold, in turn, is filled with Rosenberg-type periodic orbits.

In a non-conservative setting, this geometrical relationship between the two classic NNM concepts no longer holds, as periodic orbits become rare and isolated in the phase space, whereas infinitely many invariant manifolds tangent to each two-dimensional modal subspace will exist. A unified approach has been proposed by Haller and Ponsioen [9] to clarify the relationship between the Rosenberg and Shaw—Pierre NNM concepts. Specifically, [9] defines a nonlinear normal mode simply as a recurrent motion with finitely

*Corresponding author.

Email addresses: stenp@ethz.ch (Sten Ponsioen), ptiemo@student.ethz.ch (Tiemo Pedergnana), georgehaller@ethz.ch (George Haller)

many frequencies. Included in this theory is a trivial NNM or fixed point (no frequencies), a periodic NNM (the frequencies are rationally commensurate, as for a Rosenberg-type periodic orbit) and a quasiperiodic NNM (the frequencies are rationally incommensurate, with the orbit filling an invariant torus).

Using this NNM definition, Haller and Ponsioen [9] define a spectral submanifold (SSM) as the smoothest invariant manifold tangent to a modal subspace of a NNM. They then invoke rigorous existence, uniqueness and persistence results for autonomous and non-autonomous SSMs, providing an exact mathematical foundation for constructing nonlinear reduced-order models over appropriately chosen spectral subspaces. These models are obtained by reducing the full dynamics to the exactly invariant SSM surfaces, tangent to those subspaces.

More recently, Szalai et al. [10] have shown that the dynamics on a single-mode SSM can be seen as a nonlinear extension of the linear dynamics of the underlying modal subspace, making it possible to extract the *backbone curve*, defined as a graph plotting the instantaneous amplitude of vibration as a function of the instantaneous frequency of vibration. This approach to backbone-curve computations assumes that the Lyapunov subcenter-manifold perturbs smoothly to a unique SSM under appropriate non-resonance conditions and under small enough damping, which is consistent with the numerical observations as shown by Kerschen et al. [11], Peeters et al. [12] and Szalai et al. [10].

Computing invariant manifolds tangent to modal subspaces in realistic applications has been a challenge. Prior approaches have mostly focussed on solving the invariance equations that such manifolds have to satisfy (Blanc et al. [13], Pesheck et al. [14] and Renson et al. [15]). These invariance equations have infinitely many solutions, out of which the numerical approaches employed by different authors selected one particular solution. In contrast, the SSM theory employed here guarantees a unique solution that can be approximated with arbitrary high precision via the parameterization method of Cabré et al. [16, 17, 18]. In the present work, we describe an automated computational algorithm for two-dimensional SSMs constructed over two-dimensional modal subspaces. This algorithm¹ allows us to compute the SSMs, their reduced dynamics and associated backbone curves to arbitrary orders of accuracy, limited only by available memory. An important feature of the algorithm is a direct a posteriori estimation of the error in computing the SSM at a given approximation order. This error estimate measures directly the extend to which the SSM is invariant. If the error is unsatisfactory, the user can select higher order approximations until the error falls below a required bound.

In technical terms, we construct the SSMs as embeddings of the modal subspaces into the phase space of the mechanical system, as required by the parameterization method (Cabré et al. [16, 17, 18]). A major advantage compared to most earlier calculations (Haller and Ponsioen [9]) is that the parameterized construction of SSMs does not break down when the SSM folds over the underlying modal subspace. Another advantage of the method is its suitability for algorithmic implementations for arbitrary orders of accuracy in arbitrary dimensions. For applications of the parameterization method to other types of dynamical systems, we refer the reader to the work of Haro et al. [19], van den Berg and Mireles James [20] and Mireles James [21].

2. System set-up

We consider n -degree-of-freedom, autonomous mechanical systems of the form

$$\mathbf{M}\ddot{\mathbf{y}} + \mathbf{C}\dot{\mathbf{y}} + \mathbf{K}\mathbf{y} + \mathbf{f}(\mathbf{y}, \dot{\mathbf{y}}) = \mathbf{0}, \quad \mathbf{f}(\mathbf{y}, \dot{\mathbf{y}}) = \mathcal{O}\left(|\mathbf{y}|^2, |\mathbf{y}||\dot{\mathbf{y}}|, |\dot{\mathbf{y}}|^2\right), \quad (1)$$

where $\mathbf{y} \in \mathbb{R}^n$ is the generalized position vector; $\mathbf{M} = \mathbf{M}^T \in \mathbb{R}^{n \times n}$ is the positive definite mass matrix; $\mathbf{C} = \mathbf{C}^T \in \mathbb{R}^{n \times n}$ is the damping matrix; $\mathbf{K} = \mathbf{K}^T \in \mathbb{R}^{n \times n}$ is the stiffness matrix and $\mathbf{f}(\mathbf{x}, \dot{\mathbf{x}})$ denotes all the nonlinear terms in the system. These nonlinearities are assumed to be of class C^r in $(\mathbf{x}, \dot{\mathbf{x}})$, with $r \in \mathbb{N}^+ \cup \{\infty, a\}$. Here $r \in \mathbb{N}^+$ refers to finite differentiability, $r = \infty$ refers to infinite differentiability, and $r = a$ refer to analyticity, all three of which are allowed in our treatment.

¹SSMtool is available at: www.georgehaller.com

System (1) can be transformed into a set of $2n$ first-order ordinary differential equations by introducing a change of variables $\mathbf{x}_1 = \mathbf{y}$, $\mathbf{x}_2 = \dot{\mathbf{y}}$, with $\mathbf{x} = (\mathbf{x}_1, \mathbf{x}_2) \in \mathbb{R}^{2n}$, which gives,

$$\dot{\mathbf{x}} = \begin{pmatrix} \mathbf{0} & \mathbf{I} \\ -\mathbf{M}^{-1}\mathbf{K} & -\mathbf{M}^{-1}\mathbf{C} \end{pmatrix} \mathbf{x} + \begin{pmatrix} \mathbf{0} \\ -\mathbf{M}^{-1}\mathbf{f}(\mathbf{x}_1, \mathbf{x}_2) \end{pmatrix} = \mathbf{A}\mathbf{x} + \mathbf{F}(\mathbf{x}), \quad (2)$$

$$\mathbf{x} \in \mathbb{R}^{2n}, \quad \mathbf{F}(\mathbf{x}) = \mathcal{O}(|\mathbf{x}|^2).$$

The transformed system (2) has a fixed point at $\mathbf{x} = \mathbf{0}$, $\mathbf{A} \in \mathbb{R}^{2n \times 2n}$ is a constant matrix and $\mathbf{F}(\mathbf{x})$ is a class C^r function containing all the nonlinearities. Note that the inverse of the mass matrix is well-defined because \mathbf{M} is assumed positive definite.

The linearized part of (2) is

$$\dot{\mathbf{x}} = \mathbf{A}\mathbf{x}, \quad (3)$$

where the matrix \mathbf{A} has $2n$ eigenvalues $\lambda_k \in \mathbb{C}$ for $k = 1, \dots, 2n$. Counting multiplicities, we sort these eigenvalues based on their real parts in the decreasing order,

$$\operatorname{Re}(\lambda_{2n}) \leq \operatorname{Re}(\lambda_{2n-1}) \leq \dots \leq \operatorname{Re}(\lambda_1) < 0, \quad (4)$$

assuming that the real part of each eigenvalue is less than zero and hence the fixed point is asymptotically stable. We further assume that the constant matrix \mathbf{A} is semisimple, which implies that the algebraic multiplicity of each λ_k is equal to its geometric multiplicity, i.e. $\operatorname{alg}(\lambda_k) = \operatorname{geo}(\lambda_k)$. We can therefore identify $2n$ linearly independent eigenvectors $\mathbf{v}_k \in \mathbb{C}^{2n}$, with $k = 1, \dots, 2n$, each spanning a real eigenspace $E_k \subset \mathbb{R}^{2n}$ with $\dim(E_k) = 2 \times \operatorname{alg}(\lambda_k)$ in case $\operatorname{Im}(\lambda_k) \neq 0$, or $\dim(E_k) = \operatorname{alg}(\lambda_k)$ in case $\operatorname{Im}(\lambda_k) = 0$.

3. Spectral submanifolds for continuous mechanical systems

As \mathbf{A} is semisimple, the linear part of system (2) can be diagonalized by introducing a linear change of coordinates $\mathbf{x} = \mathbf{T}\mathbf{q}$, with $\mathbf{T} = [\mathbf{v}_{j_1}, \mathbf{v}_{j_2}, \dots, \mathbf{v}_{j_{2n}}] \in \mathbb{C}^{2n \times 2n}$ and $\mathbf{q} \in \mathbb{C}^{2n}$,

$$\dot{\mathbf{q}} = \mathbf{T}^{-1}\mathbf{A}\mathbf{T}\mathbf{q} + \mathbf{T}^{-1}\mathbf{F}(\mathbf{T}\mathbf{q}) = \underbrace{\operatorname{diag}(\lambda_{j_1}, \lambda_{j_2}, \dots, \lambda_{j_{2n}})}_{\mathbf{\Lambda}} \mathbf{q} + \underbrace{\mathbf{T}^{-1}\mathbf{F}(\mathbf{T}\mathbf{q})}_{\mathbf{G}(\mathbf{q})} = \mathbf{\Lambda}\mathbf{q} + \mathbf{G}(\mathbf{q}). \quad (5)$$

We now seek a two-dimensional modal subspace $\mathcal{E} = \operatorname{span}\{\mathbf{v}_{j_1}, \mathbf{v}_{j_2}\} \subset \mathbb{C}^{2n}$, with $\mathbf{v}_{j_2} = \bar{\mathbf{v}}_{j_1}$. Note that \mathbf{v}_{j_1} and \mathbf{v}_{j_2} are purely real if $\lambda_{j_1}, \lambda_{j_2} \in \mathbb{R}$, in which case \mathcal{E} corresponds to either a single critically damped mode ($\lambda_{j_1} = \lambda_{j_2}$), or to two overdamped modes ($\lambda_{j_1} \neq \lambda_{j_2}$). In contrast, if $\lambda_{j_1}, \bar{\lambda}_{j_2} \in \mathbb{C}$ with $\operatorname{Im} \lambda_{j_1} \neq 0$, then \mathcal{E} corresponds to a single underdamped mode.

The remaining linearly independent eigenvectors $\mathbf{v}_{j_3}, \dots, \mathbf{v}_{j_{2n}}$ span a complex subspace $\mathcal{C} \subset \mathbb{C}^{2n}$ such that the full phase space of (5) can be expressed as the direct sum

$$\mathbb{C}^{2n} = \mathcal{E} \oplus \mathcal{C}. \quad (6)$$

The diagonal matrix $\mathbf{\Lambda}$ is the representation of the linear matrix \mathbf{A} with respect to this decomposition, which we can also write as

$$\mathbf{\Lambda} = \begin{bmatrix} \mathbf{\Lambda}_{\mathcal{E}} & \mathbf{0} \\ \mathbf{0} & \mathbf{\Lambda}_{\mathcal{C}} \end{bmatrix}, \quad \operatorname{Spect}(\mathbf{\Lambda}_{\mathcal{E}}) = \{\lambda_{j_1}, \lambda_{j_2}\}, \quad \operatorname{Spect}(\mathbf{\Lambda}_{\mathcal{C}}) = \{\lambda_{j_3}, \dots, \lambda_{j_{2n}}\}, \quad (7)$$

with $\mathbf{\Lambda}_{\mathcal{E}} = \operatorname{diag}(\lambda_{j_1}, \lambda_{j_2})$ and $\mathbf{\Lambda}_{\mathcal{C}} = \operatorname{diag}(\lambda_{j_3}, \dots, \lambda_{j_{2n}})$.

Following the work of Haller and Ponsioen [9], we now define a spectral submanifold of the nonlinear system (5) as an invariant manifold tangent to the spectral subspace \mathcal{E} .

Definition 1. A *spectral submanifold* (SSM), $\mathcal{W}(\mathcal{E})$, corresponding to a spectral subspace \mathcal{E} of $\mathbf{\Lambda}$ is an invariant manifold of the dynamical system (5) such that

- (i) $\mathcal{W}(\mathcal{E})$ is tangent to \mathcal{E} and has the same dimension as \mathcal{E} .
- (ii) $\mathcal{W}(\mathcal{E})$ is strictly smoother than any other invariant manifold satisfying (i).

We define the *outer spectral quotient* $\sigma_{\text{out}}(\mathcal{E})$ as the positive integer

$$\sigma_{\text{out}}(\mathcal{E}) = \text{Int} \left[\frac{\min_{\lambda \in \text{Spect}(\mathbf{\Lambda}_C) \setminus \mathcal{E}} \text{Re} \lambda}{\max_{\lambda \in \text{Spect}(\mathbf{\Lambda}_C) \cap \mathcal{E}} \text{Re} \lambda} \right] \in \mathbb{N}^+. \quad (8)$$

Which is the integer part of the ratio between the strongest decay rate of the linearized oscillations outside \mathcal{E} and the weakest decay rate of the linearized oscillations inside \mathcal{E} . As we will see shortly, $\sigma_{\text{out}}(\mathcal{E})$ determines the smoothness class in which $\mathcal{W}(\mathcal{E})$ turns out to be unique.

To state the main results on SSMs from Haller and Ponsioen [9], we need the following two assumptions:

- (A1) $\sigma_{\text{out}}(\mathcal{E}) \leq r$,
- (A2) The *outer* non-resonance conditions

$$a\lambda_{j_1} + b\lambda_{j_2} \neq \lambda_l, \quad \forall \lambda_l \in \text{Spect}(\mathbf{\Lambda}_C). \quad (9)$$

hold for all positive integers a and b satisfying $2 \leq a + b \leq \sigma_{\text{out}}(\mathcal{E})$.

Under these assumptions, we have the following main result on an SSM tangent to the modal subspace \mathcal{E} in system (5).

Theorem 1

- (i) There exist a two-dimensional SSM, $\mathcal{W}(\mathcal{E})$, that is tangent to the spectral subspace \mathcal{E} at the fixed point $\mathbf{q} = \mathbf{0}$.
- (ii) $\mathcal{W}(\mathcal{E})$ is of class C^r and is unique among all class $C^{\sigma_{\text{out}}(\mathcal{E})+1}$ two-dimensional invariant manifolds that are tangent to \mathcal{E} at $\mathbf{q} = \mathbf{0}$.
- (iii) $\mathcal{W}(\mathcal{E})$ can be parameterized over an open set $\mathcal{U} \subset \mathbb{C}^2$ via the map

$$\mathbf{W} : \mathcal{U} \subset \mathbb{C}^2 \rightarrow \mathbb{C}^{2n}, \quad (10)$$

into the phase space of system (5).

- (iv) There exist a C^r polynomial function $\mathbf{R} : \mathcal{U} \rightarrow \mathcal{U}$ satisfying the following invariance relationship

$$\mathbf{\Lambda} \mathbf{W} + \mathbf{G} \circ \mathbf{W} = \nabla \mathbf{W} \mathbf{R}, \quad (11)$$

such that the reduced dynamics on the SSM can be expressed as

$$\dot{\mathbf{z}} = \mathbf{R}(\mathbf{z}), \quad \mathbf{R}(\mathbf{0}) = \mathbf{0}, \quad \nabla \mathbf{R}(\mathbf{0}) = \mathbf{\Lambda}_\mathcal{E} = \begin{bmatrix} \lambda_{j_1} & 0 \\ 0 & \lambda_{j_2} \end{bmatrix}, \quad \mathbf{z} = (z_{j_1}, z_{j_2}) \in \mathcal{U}. \quad (12)$$

- (v) If the *inner* non-resonance conditions

$$a\lambda_{j_1} + b\lambda_{j_2} \neq \lambda_{j_i}, \quad i = 1, 2 \quad (13)$$

hold for all positive integers a and b with

$$2 \leq a + b \leq \sigma_{\text{in}}(\mathcal{E}) = \text{Int} \left[\frac{\min_{\lambda \in \text{Spect}(\Lambda_{\mathcal{E}})} \text{Re} \lambda}{\max_{\lambda \in \text{Spect}(\Lambda_{\mathcal{E}})} \text{Re} \lambda} \right] \in \mathbb{N}^+,$$

then the mapping \mathbf{W} can be chosen in such a way that $\mathbf{R}(\mathbf{z})$ does not contain the terms $z_{j_1}^a z_{j_2}^b$. In particular, if no inner resonances arise, then the reduced dynamics on the SSM can be linearized.

The proof of Theorem 1 can be found in the work of Haller and Ponsioen [9], which is based on the more abstract results of Cabré et al. [16, 17, 18] for mappings on Banach spaces.

4. SSM computation

In this section we show how the parameterized spectral submanifolds are approximated, around a fixed point, using polynomials. We express $\mathbf{W}(\mathbf{z})$, $\mathbf{R}(\mathbf{z})$ and $\mathbf{G}(\mathbf{q})$ as multivariate polynomial functions, which is done by using the Kronecker product. Substituting the expressions in the invariance equation (11), we obtain, for each order, a linear system of equations that can be solved under appropriate non-resonance conditions. For a different application of the parameterization method, we refer to the work of Mireles James [21]. Where the parameterization method is used for approximating (un)stable manifolds of one parameter families of analytic dynamical systems, by using polynomials. For a more elaborate discussion about the numerical computation of the coefficients of higher order power series expansions of parameterized invariant manifolds around a fixed point of an elementary vector field, where the coefficients of the power series expansions are obtained using methods of Automatic Differentiation, we refer to Haro et al. [19].

4.1. The Kronecker product

We now describe a computational algorithm for constructing the mapping $\mathbf{W}(\mathbf{z})$ in (10) that maps $\mathcal{U} \subset \mathbb{C}^2$ into the phase space of system (2), and the reduced dynamics $\mathbf{R}(\mathbf{z})$ in (12). To handle the polynomial calculations arising in the algorithm efficiently, we first need to recall the notion and some properties of the Kronecker product [22].

Definition 2. Let $\mathbf{A} \in \mathbb{C}^{m \times n}$, $\mathbf{B} \in \mathbb{C}^{p \times q}$. Then we define the Kronecker product of \mathbf{A} and \mathbf{B} as

$$\mathbf{A} \otimes \mathbf{B} = \begin{bmatrix} a_{11}\mathbf{B} & \cdots & a_{1n}\mathbf{B} \\ \vdots & \ddots & \vdots \\ a_{m1}\mathbf{B} & \cdots & a_{mn}\mathbf{B} \end{bmatrix} \in \mathbb{C}^{mp \times nq}. \quad (14)$$

In accordance with Definition 2, the Kronecker product of two vectors $\mathbf{x} \in \mathbb{C}^m$ and $\mathbf{y} \in \mathbb{C}^n$ is given by the vector

$$\mathbf{x} \otimes \mathbf{y} = \begin{bmatrix} x_1\mathbf{y} \\ \vdots \\ x_m\mathbf{y} \end{bmatrix} = [x_1y_1 \cdots x_1y_n \cdots x_my_1 \cdots x_my_n]^T \in \mathbb{C}^{mn}, \quad (15)$$

or equivalently, written in index notation,

$$\mathbf{x} \otimes \mathbf{y} = \sum_{i=1}^m \sum_{j=1}^n x_i y_j \mathbf{e}_i^x \otimes \mathbf{e}_j^y, \quad (16)$$

where $\mathbf{e}_i^x \in \mathbb{C}^m$ and $\mathbf{e}_j^y \in \mathbb{C}^n$ are basis vectors containing a one in their i^{th} and j^{th} entries, respectively, and zeros elsewhere. Differentiating equation (16) with respect to time yields

$$\frac{d}{dt}(\mathbf{x} \otimes \mathbf{y}) = \frac{d}{dt}(x_i y_j \mathbf{e}_i^x \otimes \mathbf{e}_j^y) = \dot{x}_i y_j \mathbf{e}_i^x \otimes \mathbf{e}_j^y + x_i \dot{y}_j \mathbf{e}_i^x \otimes \mathbf{e}_j^y = \dot{\mathbf{x}} \otimes \mathbf{y} + \mathbf{x} \otimes \dot{\mathbf{y}}. \quad (17)$$

which is simply the product rule. By using the same reasoning, one shows that the product rule also applies to the time derivative of the Kronecker product of multiple vectors. We will use the shorthand notation $\mathbf{z}^{\otimes i}$ defined as

$$\mathbf{z}^{\otimes i} = \begin{cases} \mathbf{z} & \text{for } i = 1. \\ \underbrace{\mathbf{z} \otimes \mathbf{z} \otimes \cdots \otimes \mathbf{z}}_{i \text{ times}} & \text{for } i > 1. \end{cases} \quad (18)$$

For subsequent derivations, we will make use of several properties of the Kronecker product, which we list in Appendix A for convenience.

We Taylor expand $\mathbf{W}(\mathbf{z})$ and $\mathbf{R}(\mathbf{z})$ and express them as multivariate polynomial functions

$$\mathbf{W}(\mathbf{z}) = \sum_{i=1}^{n_w} \mathbf{W}_i \mathbf{z}^{\otimes i} = \mathbf{W}_1 \mathbf{z} + \mathbf{W}_2 \mathbf{z} \otimes \mathbf{z} + \mathbf{W}_3 \mathbf{z} \otimes \mathbf{z} \otimes \mathbf{z} + \dots, \quad \mathbf{W}_i \in \mathbb{C}^{2n \times 2^i}, \quad \mathbf{z} \in \mathbb{C}^2, \quad (19)$$

$$\mathbf{R}(\mathbf{z}) = \sum_{i=1}^{n_w} \mathbf{R}_i \mathbf{z}^{\otimes i} = \mathbf{R}_1 \mathbf{z} + \mathbf{R}_2 \mathbf{z} \otimes \mathbf{z} + \mathbf{R}_3 \mathbf{z} \otimes \mathbf{z} \otimes \mathbf{z} + \dots, \quad \mathbf{R}_i \in \mathbb{C}^{2 \times 2^i}, \quad \mathbf{z} \in \mathbb{C}^2, \quad (20)$$

with $n_w \geq \sigma_{\text{out}}(\mathcal{E}) + 1$ denoting the order of the SSM expansion. We also Taylor expand the nonlinear part of our dynamical system (5) up to order n_w , around the fixed point $\mathbf{q} = \mathbf{0}$, such that we can represent the nonlinearities, in a fashion similar to equations (19) and (20), as

$$\mathbf{G}(\mathbf{q}) = \sum_{i=2}^{\Gamma} \mathbf{G}_i \mathbf{q}^{\otimes i} = \mathbf{G}_2 \mathbf{q} \otimes \mathbf{q} + \mathbf{G}_3 \mathbf{q} \otimes \mathbf{q} \otimes \mathbf{q} + \dots, \quad \mathbf{G}_i \in \mathbb{C}^{2n \times (2n)^i}, \quad \mathbf{q} \in \mathbb{C}^{2n}, \quad (21)$$

with Γ denoting the maximum order of nonlinearity considered.

By construction, the vector $\mathbf{q}^{\otimes i}$ will have redundant terms along its elements, and hence \mathbf{G}_i will have infinitely many possible representations at the i^{th} order in equation (5). The redundancy in $\mathbf{q}^{\otimes i}$ allows us to introduce constraints between the different coefficients that are related to the same monomial term. We can always set these constraints such that $\mathbf{G}(\mathbf{q})$ will represent the $2n$ -dimensional polynomial vector $\mathbf{T}^{-1}\mathbf{F}(\mathbf{T}\mathbf{q})$. For more detail, we refer the reader to Appendix C.

4.2. The coefficient equations

We recall here the diagonalized dynamical system (5)

$$\dot{\mathbf{q}} = \Lambda \mathbf{q} + \mathbf{G}(\mathbf{q}). \quad (22)$$

Substituting $\mathbf{q} = \mathbf{W}(\mathbf{z})$ on the right-hand side of equation (22), then differentiating $\mathbf{q} = \mathbf{W}(\mathbf{z})$ with respect to time and substituting the result $\dot{\mathbf{q}} = \nabla \mathbf{W}(\mathbf{z}) \dot{\mathbf{z}}$ on the left-hand side of equation (22), we obtain the invariance relation (11) in the form

$$\begin{aligned} & \mathbf{W}_1 \mathbf{R}(\mathbf{z}) + \mathbf{W}_2 (\mathbf{R}(\mathbf{z}) \otimes \mathbf{z} + \mathbf{z} \otimes \mathbf{R}(\mathbf{z})) \\ & + \mathbf{W}_3 (\mathbf{R}(\mathbf{z}) \otimes \mathbf{z} \otimes \mathbf{z} + \mathbf{z} \otimes \mathbf{R}(\mathbf{z}) \otimes \mathbf{z} + \mathbf{z} \otimes \mathbf{z} \otimes \mathbf{R}(\mathbf{z})) + \dots \\ & + \mathbf{W}_k (\mathbf{R}(\mathbf{z}) \otimes \mathbf{z}^{\otimes k-1} + \sum_{j=1}^{k-2} (\mathbf{z}^{\otimes j} \otimes \mathbf{R}(\mathbf{z}) \otimes \mathbf{z}^{\otimes k-j-1}) + \mathbf{z}^{\otimes k-1} \otimes \mathbf{R}(\mathbf{z})) \\ & = \Lambda \mathbf{W}(\mathbf{z}) + \mathbf{G}_2 \mathbf{W}(\mathbf{z})^{\otimes 2} + \dots + \mathbf{G}_\Gamma \mathbf{W}(\mathbf{z})^{\otimes \Gamma}, \end{aligned} \quad (23)$$

for $k = \{2, \dots, n_w\}$. The time derivative of $\mathbf{q} = \mathbf{W}(\mathbf{z}) = \sum_i \mathbf{W}_i \mathbf{z}^{\otimes i}$ can be expressed, using the product rule for the Kronecker product of vectors, as

$$\dot{\mathbf{q}} = \mathbf{W}_1 \dot{\mathbf{z}} + \mathbf{W}_2 (\dot{\mathbf{z}} \otimes \mathbf{z} + \mathbf{z} \otimes \dot{\mathbf{z}}) + \mathbf{W}_3 (\dot{\mathbf{z}} \otimes \mathbf{z} \otimes \mathbf{z} + \mathbf{z} \otimes \dot{\mathbf{z}} \otimes \mathbf{z} + \mathbf{z} \otimes \mathbf{z} \otimes \dot{\mathbf{z}}) + \dots \quad (24)$$

Substituting $\dot{\mathbf{z}} = \mathbf{R}(\mathbf{z})$ into (24), we precisely obtain the left-hand side of equation (23). Rewriting equation (23) and collecting terms of equal power $\mathbf{z}^{\otimes i}$ for $i = \{1, \dots, n_w\}$, we obtain, for $i = 1$,

$$\underbrace{\begin{bmatrix} \Lambda_{\mathcal{E}} & \mathbf{0} \\ \mathbf{0} & \Lambda_{\mathcal{C}} \end{bmatrix}}_{\Lambda} \mathbf{W}_1 = \mathbf{W}_1 \mathbf{R}_1. \quad (25)$$

From (12), we then require that $\nabla \mathbf{R}(\mathbf{0}) = \Lambda_{\mathcal{E}} = \mathbf{R}_1$. Therefore, equation (25) will be satisfied if we set $\mathbf{W}_1 \in \mathbb{C}^{2n \times 2}$ equal to

$$\mathbf{W}_1 = \begin{bmatrix} 1 & 0 \\ 0 & 1 \\ 0 & 0 \\ \vdots & \vdots \\ 0 & 0 \end{bmatrix}. \quad (26)$$

For $2 \leq i \leq n_w$ we have

$$\begin{aligned} \Lambda \mathbf{W}_i - \mathbf{W}_i \sum_{|\mathbf{s}|=1}^{\tilde{\Lambda}_{\mathcal{E},i}} \Lambda_{\mathcal{E}}^{s_1} \otimes \dots \otimes \Lambda_{\mathcal{E}}^{s_i} &= \mathbf{W}_1 \mathbf{R}_i + \sum_{m=2}^{i-1} \mathbf{W}_m \sum_{|\mathbf{p}|=1} \mathbf{R}_{i+1-m}^{p_1} \otimes \dots \otimes \mathbf{R}_{i+1-m}^{p_m} \\ &\quad - \mathbf{G}_i \mathbf{W}_1^{\otimes i} - \sum_{m=2}^{i-1} \mathbf{G}_m \sum_{|\mathbf{r}|=i} \mathbf{W}_{r_1} \otimes \dots \otimes \mathbf{W}_{r_m}, \end{aligned} \quad (27)$$

where we make use of multi-index notation for $\mathbf{s} = \{s_1, \dots, s_i\} \in \mathbb{N}^i$, $\mathbf{p} = \{p_1, \dots, p_m\} \in \mathbb{N}^m$ and $\mathbf{r} = \{r_1, \dots, r_m\} \in \mathbb{N}^m$. The notation $\Lambda_{\mathcal{E}}^{s_j}$ is used to indicate that the matrix $\Lambda_{\mathcal{E}}$ is taken to the power $s_j \in \mathbb{N}$, where the zeroth power will simply return the identity matrix of the same dimension as $\Lambda_{\mathcal{E}}$. Note that we also adopt the same notation for $\mathbf{R}_{i+1-m} \in \mathbb{C}^{2 \times 2^{i+1-m}}$, where we set $\mathbf{R}_{i+1-m}^0 \triangleq \mathbf{I} \in \mathbb{R}^{2 \times 2}$.

The right hand side of equation (27) consists of the lower-order terms \mathbf{W}_j for $2 \leq j < i - 1$, which are known for the current order i . The term \mathbf{R}_i represents the coefficient matrix corresponding to the i^{th} -order of the polynomial $\mathbf{R}(\mathbf{z})$. This polynomial depends on the preferred style of parameterization and will be chosen to remove near-inner resonances from the SSM expressions, as explained later in section 5. The matrices \mathbf{G}_j , for $2 \leq j \leq i$, are known by definition because they represent the nonlinearities of system (5).

4.2.1. Partitioning the coefficient equations

Due to the diagonal structure of Λ , we can partition equation (27) into the two separate matrix equations

$$\Lambda_{\mathcal{E}} \mathbf{W}_i^{\mathcal{E}} - \mathbf{W}_i^{\mathcal{E}} \tilde{\Lambda}_{\mathcal{E},i} = \mathbf{R}_i + \mathbf{B}_i^{\mathcal{E}}, \quad (28)$$

$$\Lambda_{\mathcal{C}} \mathbf{W}_i^{\mathcal{C}} - \mathbf{W}_i^{\mathcal{C}} \tilde{\Lambda}_{\mathcal{E},i} = \mathbf{B}_i^{\mathcal{C}}, \quad (29)$$

where \mathbf{W}_i is partitioned as

$$\mathbf{W}_i = \begin{bmatrix} \mathbf{W}_i^{\mathcal{E}} \\ \mathbf{W}_i^{\mathcal{C}} \end{bmatrix} \in \mathbb{C}^{2n \times 2^i}, \quad \mathbf{W}_i^{\mathcal{E}} \in \mathbb{C}^{2 \times 2^i}, \quad \mathbf{W}_i^{\mathcal{C}} \in \mathbb{C}^{(2n-2) \times 2^i}. \quad (30)$$

The matrices $\mathbf{B}_i^{\mathcal{E}} \in \mathbb{C}^{2 \times 2^i}$ and $\mathbf{B}_i^{\mathcal{C}} \in \mathbb{C}^{(2n-2) \times 2^i}$ are such that

$$\begin{bmatrix} \mathbf{B}_i^{\mathcal{E}} \\ \mathbf{B}_i^{\mathcal{C}} \end{bmatrix} = \sum_{m=2}^{i-1} \mathbf{W}_m \sum_{|\mathbf{p}|=1} \mathbf{R}_{i+1-m}^{p_1} \otimes \dots \otimes \mathbf{R}_{i+1-m}^{p_m} - \mathbf{G}_i \mathbf{W}_1^{\otimes i} - \sum_{m=2}^{i-1} \mathbf{G}_m \sum_{|\mathbf{r}|=i} \mathbf{W}_{r_1} \otimes \dots \otimes \mathbf{W}_{r_m}. \quad (31)$$

Equations (28) and (29) are also known as the Sylvester equations [22], having the unknown coefficient matrices $\mathbf{W}_i^\mathcal{E}$ and $\mathbf{W}_i^\mathcal{C}$. Using the Kronecker product and the vectorization operation

$$\text{vec}(\mathbf{A}) = \text{vec}([\mathbf{a}_1 \mathbf{a}_2 \dots \mathbf{a}_n]) = \begin{bmatrix} \mathbf{a}_1 \\ \vdots \\ \mathbf{a}_n \end{bmatrix} \in \mathbb{C}^{mn}, \quad \mathbf{A} \in \mathbb{C}^{m \times n}, \quad (32)$$

with $\mathbf{a}_1, \dots, \mathbf{a}_n$ denoting the column vectors of \mathbf{A} , we rewrite equation (28) and equation (29) as

$$\underbrace{(\mathbf{I}_{2^i \times 2^i} \otimes \Lambda_\mathcal{E} - \tilde{\Lambda}_{\mathcal{E},i}^T \otimes \mathbf{I}_{2 \times 2})}_{\Theta_i^\mathcal{E}} \text{vec}(\mathbf{W}_i^\mathcal{E}) = \text{vec}(\mathbf{R}_i) + \text{vec}(\mathbf{B}_i^\mathcal{E}). \quad (33)$$

$$\underbrace{(\mathbf{I}_{2^i \times 2^i} \otimes \Lambda_\mathcal{C} - \tilde{\Lambda}_{\mathcal{E},i}^T \otimes \mathbf{I}_{(2n-2) \times (2n-2)})}_{\Theta_i^\mathcal{C}} \text{vec}(\mathbf{W}_i^\mathcal{C}) = \text{vec}(\mathbf{B}_i^\mathcal{C}). \quad (34)$$

4.2.2. Invertibility of $\Theta_i^\mathcal{E}$ and $\Theta_i^\mathcal{C}$

Finding a unique solution for $\mathbf{W}_i^\mathcal{C}$ in equation (34) for a nonzero right-hand side requires the matrix $\Theta_i^\mathcal{C}$ to be non-singular. If, however, $\Theta_i^\mathcal{E}$ is singular, which arises from exact inner resonances, it suffices for the vectorized solution for $\mathbf{W}_i^\mathcal{E}$ to be in the kernel of $\Theta_i^\mathcal{E}$. We can ensure this by choosing $\text{vec}(\mathbf{R}_i)$ such that the right-hand side of equation (33) is zero. To carry out all this, we need to find the eigenvalues of $\Theta_i^\mathcal{E}$ and $\Theta_i^\mathcal{C}$.

It can be shown [22] that for a matrix $\mathbf{A} \in \mathbb{C}^{n \times n}$, with the eigenvalues λ_i and a matrix $\mathbf{B} \in \mathbb{C}^{m \times m}$ with eigenvalues μ_j , the matrix $\mathbf{I}_{m \times m} \otimes \mathbf{A} - \mathbf{B} \otimes \mathbf{I}_{n \times n}$ has the mn eigenvalues

$$\lambda_1 - \mu_1, \dots, \lambda_1 - \mu_m, \lambda_2 - \mu_1, \dots, \lambda_2 - \mu_m, \dots, \lambda_n - \mu_1, \dots, \lambda_n - \mu_m. \quad (35)$$

In the current setting of (33) and (34), we know that the eigenvalues of $\Lambda_\mathcal{E}$ and $\Lambda_\mathcal{C}$ are $\lambda_{j_1}, \lambda_{j_2}$ and $\lambda_{j_3}, \dots, \lambda_{j_{2n}}$, respectively. By further exploiting the structure of

$$\tilde{\Lambda}_{\mathcal{E},i}^T = \tilde{\Lambda}_{\mathcal{E},i} = \sum_{|\mathbf{s}|=1} \Lambda_\mathcal{E}^{s_1} \otimes \dots \otimes \Lambda_\mathcal{E}^{s_i} = \Lambda_\mathcal{E} \otimes \mathbf{I} \otimes \dots \otimes \mathbf{I} + \dots + \mathbf{I} \otimes \mathbf{I} \otimes \dots \otimes \Lambda_\mathcal{E}, \quad (36)$$

or, equivalently,

$$\tilde{\Lambda}_{\mathcal{E},i} = \text{diag}(a_1 \lambda_1 + b_1 \lambda_2, \dots, a_{2^i} \lambda_1 + b_{2^i} \lambda_2) \in \mathbb{C}^{2^i \times 2^i}, \quad (37)$$

we observe that each diagonal term of the matrix $\tilde{\Lambda}_\mathcal{E}$ for a given order i will consist of a linear combination of λ_1 and λ_2 , i.e., $a_j \lambda_1 + b_j \lambda_2$ for $j = \{1, \dots, 2^i\}$, with $a_j, b_j \in \mathbb{N}$. Now let Ω_i be a 2^i -dimensional vector containing all possible lexicographically ordered i -tuples made out of elements of the set $\{1, 2\}$, in which repetition is allowed. The multiplicity corresponding to the numbers 1 and 2, in the j^{th} element of Ω_i , will represent a_j and b_j respectively. To illustrate this, we give an example

Example 1. [Constructing the matrix $\tilde{\Lambda}_{\mathcal{E},2}$] For $i = 2$, the diagonal matrix $\tilde{\Lambda}_{\mathcal{E},2}$ is equal to

$$\begin{aligned} \tilde{\Lambda}_{\mathcal{E},2} = \Lambda_\mathcal{E} \otimes \mathbf{I} + \mathbf{I} \otimes \Lambda_\mathcal{E} &= \begin{bmatrix} \lambda_{j_1} & 0 \\ 0 & \lambda_{j_2} \end{bmatrix} \otimes \begin{bmatrix} 1 & 0 \\ 0 & 1 \end{bmatrix} + \begin{bmatrix} 1 & 0 \\ 0 & 1 \end{bmatrix} \otimes \begin{bmatrix} \lambda_{j_1} & 0 \\ 0 & \lambda_{j_2} \end{bmatrix} \\ &= \begin{bmatrix} 2\lambda_{j_1} & 0 & 0 & 0 \\ 0 & \lambda_{j_1} + \lambda_{j_2} & 0 & 0 \\ 0 & 0 & \lambda_{j_2} + \lambda_{j_1} & 0 \\ 0 & 0 & 0 & 2\lambda_{j_2} \end{bmatrix}. \end{aligned} \quad (38)$$

The four-dimensional array Ω_2 can be expressed as

$$\Omega_2 = (11, 12, 21, 22),$$

from which we obtain the coefficients (a_j, b_j) by determining the multiplicity of the numbers 1 and 2 for each element j in Ω_2 .

As $\tilde{\Lambda}_{\mathcal{E},i}$ is diagonal by construction, its eigenvalues are positioned on the diagonal and take the form of

$$a\lambda_{j_1} + b\lambda_{j_2}, \quad a, b \in \mathbb{N} : a + b = i. \quad (39)$$

We, therefore, conclude from (35) that the eigenvalues of $\Theta_i^{\mathcal{E}}$ and $\Theta_i^{\mathcal{C}}$ can be written as

$$\lambda_l - (a\lambda_{j_1} + b\lambda_{j_2}), \quad a, b \in \mathbb{N} : a + b = i, \quad \forall \lambda_l \in \text{Spect}(\Lambda_{\mathcal{E}}), \quad (40)$$

$$\lambda_l - (a\lambda_{j_1} + b\lambda_{j_2}), \quad a, b \in \mathbb{N} : a + b = i, \quad \forall \lambda_l \in \text{Spect}(\Lambda_{\mathcal{C}}). \quad (41)$$

Equations (40) and (41) lead precisely to the inner and outer non-resonance conditions (13) and (9), respectively, related to the i^{th} -order of the SSM expansion. If there exists an inner resonance in (40), for a particular order i , the matrix $\Theta_i^{\mathcal{E}}$ will be singular. This means that for a nonzero right-hand side of equation (33), there will be no solution for $\text{vec}(\mathbf{W}_i^{\mathcal{E}})$. However, we can then set \mathbf{R}_i in equation (33) equal to $-\mathbf{B}_i^{\mathcal{E}}$, which gives a zero right-hand side. As a consequence, the solution $\text{vec}(\mathbf{W}_i^{\mathcal{E}})$ has to be in the kernel of $\Theta_i^{\mathcal{E}}$, creating an opportunity to remove resonant terms in the expression for $\mathbf{W}(\mathbf{z})$. The presence of an outer resonance in (41) will result in a breakdown of the SSM. In this case, we do not have the freedom to alter the right-hand side of equation (34).

5. Reduced dynamics on the SSM

5.1. Near-inner-resonances

Based on eq. (33), the polynomial dynamics on the SSM must be parameterized as nonlinear when an inner resonance arises in the spectral subspace \mathcal{E} over which the SSM is constructed. When the eigenvalues λ_{j_1} and λ_{j_2} are complex conjugate, the inner non-resonance conditions (13) will never be violated. However, as explained by Szalai et al. [10], for a lightly damped spectral subspace corresponding to a complex pair of eigenvalues, the following near-inner-resonance conditions will always hold:

$$2\lambda_{j_1} + \bar{\lambda}_{j_1} \approx \lambda_{j_1}, \quad \lambda_{j_1} + 2\bar{\lambda}_{j_1} \approx \bar{\lambda}_{j_1}. \quad (42)$$

These near-inner-resonances, in turn, will lead to small denominators in the coefficients related to the monomial terms $z_{j_1}^2 \bar{z}_{j_1}$ and $z_{j_1} \bar{z}_{j_1}^2$ in the third-order coefficient matrix $\mathbf{W}_3^{\mathcal{E}}$ (cf. eqs. (33-34)). Such small denominators generally reduce the domain of convergence of the Taylor series we compute for $\mathbf{W}(\mathbf{z})$.

Luckily, we have the freedom to remove these resonant terms in $\mathbf{W}_3^{\mathcal{E}}$ by setting \mathbf{R}_3 on the right-hand side of equation (28) equal to $-\mathbf{B}_3^{\mathcal{E}}$. However, due to the particular diagonal structure of equation (33), it is possible to specifically remove the resonant terms $z_{j_1}^2 \bar{z}_{j_1}$ and $z_{j_1} \bar{z}_{j_1}^2$ in $\mathbf{W}_3^{\mathcal{E}}$ by only setting the coefficients in \mathbf{R}_3 related to the the resonant terms equal to the coefficients in $-\mathbf{B}_3^{\mathcal{E}}$. This corresponds to a mixed parameterization style, as explained in Haro et al. [19], which can also be applied to higher orders.

The third order near-inner-resonance condition (42) can be extended to higher-order near-inner-resonances by introducing an appropriate resonance-closeness measure

$$I(a, b, \lambda_l) = \left| \frac{\langle \mathbf{c}(a, b), \mathbf{v}_{\mathcal{E}}(\lambda_l) \rangle}{\|\mathbf{c}(a, b)\| \|\mathbf{v}_{\mathcal{E}}(\lambda_l)\|} \right| < \delta, \quad 0 < \delta \ll 1, \quad (43)$$

for δ sufficiently small, with

$$\mathbf{c}(a, b) = \begin{bmatrix} a \\ b \\ -1 \end{bmatrix}, \quad \mathbf{v}_{\mathcal{E}}(\lambda_l) = \begin{bmatrix} \lambda_{j_1} \\ \lambda_{j_2} \\ \lambda_l \end{bmatrix}, \quad a, b \in \mathbb{N}, \quad \forall \lambda_l \in \{\lambda_{j_1}, \lambda_{j_2}\}.$$

The resonance-closeness measure I takes values between $I_{\min} = 0$ and $I_{\max} = 1$. We consider δ to be small when δ is at least one order of magnitude smaller than I_{\max} . In the presence of near-inner resonances, the choice of δ affects the accuracy of the SSM and the reduced dynamics. If the observed invariance error of the SSM (cf. section 6) is unsatisfactory, δ can be increased in order to account for even weaker near-inner resonances.

In the case of an exact inner resonance, $I(a, b, \lambda_l)$ in equation (43) will be zero. Using the same measure, we can also quantify closeness to outer resonances by substituting all possible $\lambda_l \notin \{\lambda_{j_1}, \lambda_{j_2}\}$ into (43).

5.2. Instantaneous amplitude and frequency

When the chosen spectral subspace \mathcal{E} is spanned by a complex pair of eigenvectors, which in turn corresponds to a complex conjugate pair of eigenvalues λ_{j_1} and λ_{j_2} , the complex conjugate pair of coordinates z_{j_1} and $z_{j_2} = \bar{z}_{j_1}$ in the reduced dynamics $\mathbf{R}(\mathbf{z})$ can be expressed in real amplitude-phase coordinates (ρ, θ) as

$$z_{j_1} = \rho e^{i\theta}, \quad \bar{z}_{j_1} = \rho e^{-i\theta}. \quad (44)$$

Assume now that the spectral subspace \mathcal{E} has higher-order near-inner-resonances, i.e.

$$I(a, b, \lambda_{j_1}) < \delta, \quad I(b, a, \lambda_{j_2}) < \delta, \quad (a, b) \in \{(2, 1), (3, 2), (4, 3), \dots\} = S,$$

and, additionally, the coefficients in $\mathbf{B}_i^{\mathcal{E}}$ for $i = 3, 5, 7, \dots$, corresponding to the monomial terms $z_{j_1}^a \bar{z}_{j_1}^b$ and $z_{j_1}^s \bar{z}_{j_1}^r$, on the right hand side of (28) are nonzero. We then obtain the following expression for the reduced dynamics on the spectral submanifold $\mathcal{W}(\mathcal{E})$:

$$\dot{\mathbf{z}} = \mathbf{R}(\mathbf{z}) = \begin{bmatrix} \lambda_{j_1} z_{j_1} + \sum_{\forall (a,b) \in S} \gamma_{a,b} z_{j_1}^a \bar{z}_{j_1}^b \\ \bar{\lambda}_{j_1} \bar{z}_{j_1} + \sum_{\forall (a,b) \in S} \bar{\gamma}_{a,b} z_{j_1}^b \bar{z}_{j_1}^a \end{bmatrix}. \quad (45)$$

Here $\gamma_{a,b}$ depends directly on $\mathbf{B}_i^{\mathcal{E}}$, which is known for the current order i . Alternatively, $\gamma_{a,b}$ will be equal to the sum of all nonzero coefficients in \mathbf{R}_i , with $i = a + b$ corresponding to the monomial term $z_{j_1}^a \bar{z}_{j_1}^b$. Substituting equation (44) into the left- and right-hand side of equation (45) gives

$$\dot{\rho} = \operatorname{Re}(\lambda_{j_1})\rho + \sum_{\forall (a,b) \in S} \operatorname{Re}(\gamma_{a,b})\rho^{(a+b)}, \quad (46)$$

$$\omega = \dot{\theta} = \operatorname{Im}(\lambda_{j_1}) + \sum_{\forall (a,b) \in S} \operatorname{Im}(\gamma_{a,b})\rho^{(a+b-1)}. \quad (47)$$

for $\rho \neq 0$. Equation (47) determines an instantaneous frequency $\dot{\theta}$ that depends solely upon ρ . To any ρ value, we assign an instantaneous physically observable amplitude by defining

$$A(\rho) = \frac{1}{2\pi} \int_0^{2\pi} |\mathbf{T}_y \mathbf{W}(\mathbf{z}(\rho, \theta))| d\theta, \quad (48)$$

where the transformation matrix \mathbf{T}_y acts on $\mathbf{W}(\mathbf{z}(\rho, \theta))$ and hence returns physical position coordinates $\mathbf{y} \in \mathbb{R}^n$ of our mechanical system (2). Then, following the definition of Szalai et al. [10], we define a backbone curve for the reduced dynamics on the SSM to be the parameterized curve

$$\mathcal{B} = \{\omega(\rho), A(\rho)\}_{\rho \in \mathbb{R}^+}. \quad (49)$$

An illustration of how the parametrized SSM, constructed over a lightly damped spectral subspace \mathcal{E} , can be used to construct the backbone curve \mathcal{B} is shown in figure 1.

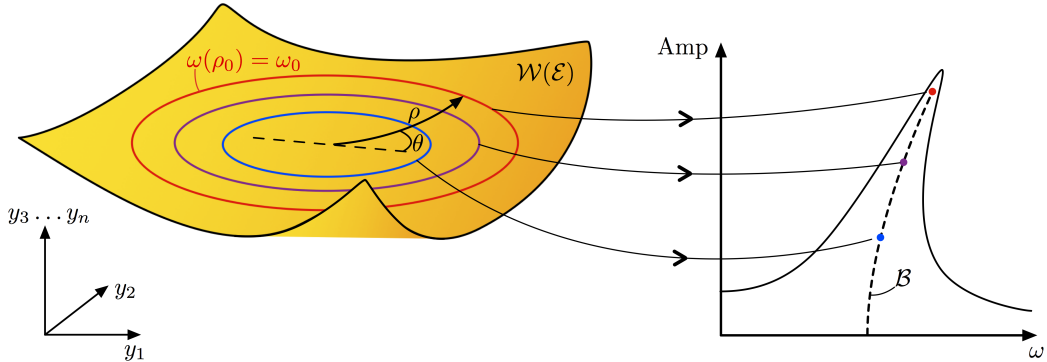


Figure 1: Illustration of the backbone curve construction using the parameterized SSM. For each fixed radius ρ_0 on the SSM, we can identify an instantaneous frequency (47). By averaging the physical coordinates over one period, evaluated on the SSM constraint to the fixed radius ρ_0 , we obtain the instantaneous amplitude (48). For each $\rho = \rho_0 \in \mathbb{R}^+$, we obtain a point of the curve \mathcal{B} , shown in the amplitude-frequency plot. The continuous black line in the amplitude-frequency plot consists out of periodic orbits of the periodically forced system for varying forcing frequency.

6. Invariance measure and order selection

As stated in Theorem 1, the unique SSM is captured and approximated by Taylor expanding up to order $\sigma_{\text{out}}(\mathcal{E}) + 1$. The outer spectral quotient σ_{out} , is defined as the integer part of the ratio between the strongest decay rate of the linearized oscillations outside \mathcal{E} and the weakest decay rate of the linearized oscillations inside \mathcal{E} . As explained by G eradin and Rixen [23], a first-order approximation of the real part of each eigenvalue of a lightly damped mechanical system, of the form (1), scales with the square of its natural eigenfrequency. This means that for a discretized non-conservative mechanical system with a high number of degrees of freedom, the order of the SSM needed to be unique can become large. An illustration of this is shown in figure 2.

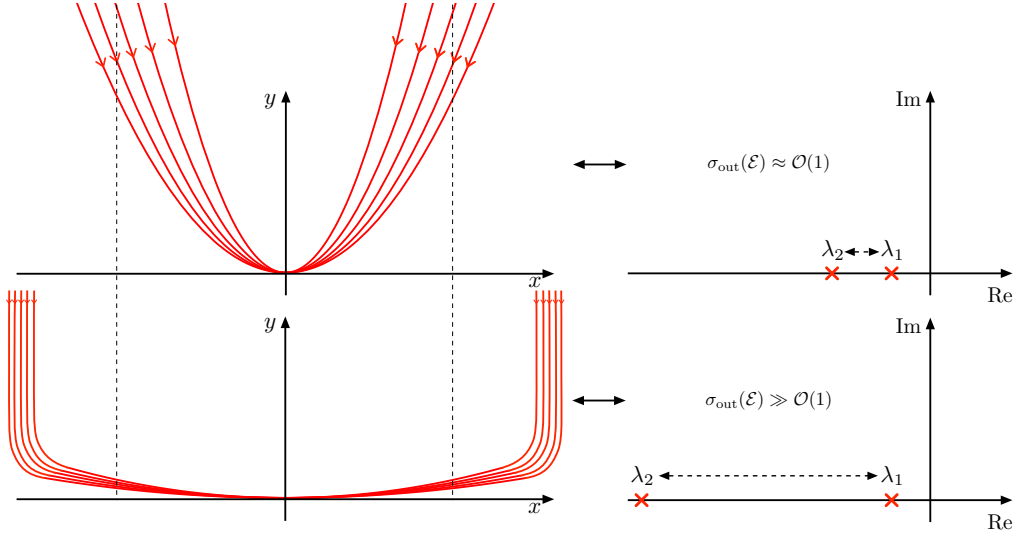


Figure 2: Illustration of a system having a low outer spectral quotient (top) and a high outer spectral quotient (bottom).

As the outer spectral quotient $\sigma_{\text{out}}(\mathcal{E})$ increases, trajectories transverse to the slow SSM die out fast compared to trajectories on the SSM, as indicated in the lower part of figure 2. This collapsing nature of the transverse trajectories makes it harder to distinguish between the unique SSM and any other two-dimensional invariant manifold tangent the same modal subspace. In order to approximate the SSMs with a large outer spectral quotient, without having to compute the SSMs up to extremely high orders, we introduce an invariance error measure, δ_{inv} , that quantifies the accuracy of the computed invariant manifolds and the reduced dynamics on them.

The invariance error measure compares trajectories of the full system \mathbf{x}_i , with trajectories of the reduced system $\tilde{\mathbf{x}}_i$. Trajectories from the full and reduced system are launched from a circle with fixed radius ρ_0 , from the origin, and integrated until the reduced trajectories cross the inner circle of radius $\rho_\epsilon < \rho_0$, therefore removing the time dependency. An illustration of this is shown in figure 3. We mathematically formalize the invariance error as follows

$$\delta_{\text{inv}} = \frac{1}{N} \sum_{i=1}^N \frac{\text{dist}(i)}{\max_{\theta \in S^1} \|\tilde{\mathbf{x}}(\rho_0, \theta)\|_2}, \quad \text{dist}(i) = \max \left\| \mathbf{x}_i|_{\rho_0}^{\rho_\epsilon} - \tilde{\mathbf{x}}_i|_{\rho_0}^{\rho_\epsilon} \right\|_2, \quad (50)$$

where we take the average of the maximum Euclidean distance between N trajectories \mathbf{x}_i and $\tilde{\mathbf{x}}_i$, for $i = 1, \dots, N$, traveling from a circle with radius ρ_0 to an inner circle with radius ρ_ϵ , and normalize the result by the maximum Euclidean distance from the origin to the circle with fixed radius ρ_0 .

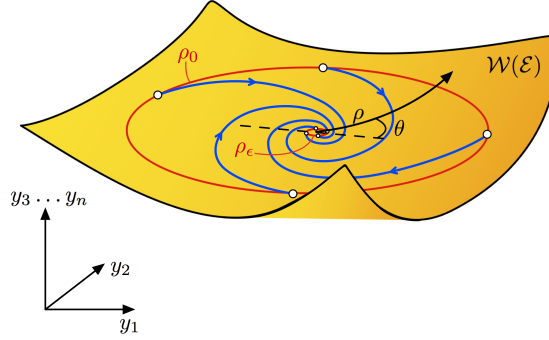


Figure 3: Illustration of the invariance error measure.

If the invariance error δ_{inv} , for a given order of the approximated SSM, is above a certain pre-specified bound, then the order of the SSM approximation has to be further increased.

7. Applications

We now apply our computational algorithm to three different mechanical systems. The numerical results and figures we show have all been generated directly by SSMtool.

7.1. The modified Shaw–Pierre example: Inner resonances

We first consider a slightly modified version of the example of Shaw and Pierre [24], shown in figure 4. The original Shaw–Pierre example involves a two-degree-of-freedom mechanical oscillator, which is modified in the current setting such that the damping matrix is proportional to the mass and stiffness matrices (also known as Rayleigh damping, see, e.g., Géradin and Rixen [23]). For this problem, the SSM coefficients have been explicitly calculated in Szalai et al. [10], up to third order.

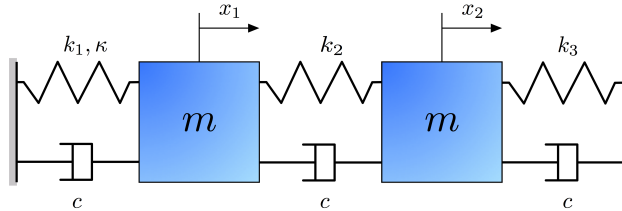


Figure 4: Two-degree-of-freedom modified Shaw–Pierre example.

For $k_1 = k_2 = k_3 = k$, the equations of motion of the system are

$$\begin{bmatrix} m & 0 \\ 0 & m \end{bmatrix} \begin{bmatrix} \ddot{x}_1 \\ \ddot{x}_2 \end{bmatrix} + \begin{bmatrix} 2c & -c \\ -c & 2c \end{bmatrix} \begin{bmatrix} \dot{x}_1 \\ \dot{x}_2 \end{bmatrix} + \begin{bmatrix} 2k & -k \\ -k & 2k \end{bmatrix} \begin{bmatrix} x_1 \\ x_2 \end{bmatrix} + \begin{bmatrix} \kappa x_1^3 \\ 0 \end{bmatrix} = \begin{bmatrix} 0 \\ 0 \end{bmatrix}, \quad (51)$$

with the linear part having the eigenvalue pairs

$$\lambda_{1,2} = -\frac{c}{2} \pm i\sqrt{k\left(1 - \frac{c^2}{4k}\right)}, \quad \lambda_{3,4} = -\frac{3c}{2} \pm i\sqrt{3k\left(1 - \frac{3c^2}{4k}\right)}, \quad (52)$$

when both linear normal modes are underdamped ($c < 2\sqrt{k/3}$) and the mass m is equal to 1 kg. As noted in Szalai et al. [10], the two spectral subspaces, \mathcal{E}_1 and \mathcal{E}_2 , corresponding to the eigenvalues $\lambda_{1,2}$ and $\lambda_{3,4}$ respectively, have the outer and inner spectral quotients

$$\sigma_{\text{out}}(\mathcal{E}_1) = \text{Int} \left[\frac{\text{Re}\lambda_3}{\text{Re}\lambda_1} \right] = 3, \quad \sigma_{\text{out}}(\mathcal{E}_2) = \left[\frac{\text{Re}\lambda_1}{\text{Re}\lambda_3} \right] = 0, \quad (53)$$

$$\sigma_{\text{in}}(\mathcal{E}_1) = \text{Int} \left[\frac{\text{Re}\lambda_1}{\text{Re}\lambda_1} \right] = 1, \quad \sigma_{\text{in}}(\mathcal{E}_2) = \left[\frac{\text{Re}\lambda_3}{\text{Re}\lambda_3} \right] = 1. \quad (54)$$

The non-resonance conditions (9) and (13) are satisfied for both of these spectral subspaces, thus, there exist two two-dimensional analytic SSMS, $\mathbf{W}(\mathcal{E}_1)$ and $\mathbf{W}(\mathcal{E}_2)$, that are unique among all C^4 and C^1 invariant manifolds tangent to \mathcal{E}_1 and \mathcal{E}_2 , respectively.

Rewriting the equations of motion (51) in first-order form, we obtain

$$\frac{d}{dt} \begin{bmatrix} x_1 \\ x_2 \\ \dot{x}_1 \\ \dot{x}_2 \end{bmatrix} = \underbrace{\begin{bmatrix} 0 & 0 & 1 & 0 \\ 0 & 0 & 0 & 1 \\ -2k & k & -2c & c \\ k & -2k & c & -2c \end{bmatrix}}_{\mathbf{A}} \begin{bmatrix} x_1 \\ x_2 \\ \dot{x}_1 \\ \dot{x}_2 \end{bmatrix} + \underbrace{\begin{bmatrix} 0 \\ 0 \\ -\kappa x_1^3 \\ 0 \end{bmatrix}}_{\mathbf{F}(\mathbf{x})}. \quad (55)$$

7.1.1. Computing $\mathbf{W}(\mathcal{E}_1)$ and $\mathbf{W}(\mathcal{E}_2)$

The spectral submanifolds, $\mathbf{W}(\mathcal{E}_1)$ and $\mathbf{W}(\mathcal{E}_2)$, will be tangent to their corresponding spectral subspaces, \mathcal{E}_1 and \mathcal{E}_2 . To compute $\mathbf{W}(\mathcal{E}_1)$, we diagonalize (55) by introducing a linear change of coordinates $\mathbf{x} = \mathbf{T}\mathbf{q}$, where the columns of \mathbf{T} contain the eigenvectors of (55), i.e.,

$$\mathbf{T} = [\mathbf{v}_1, \bar{\mathbf{v}}_1, \mathbf{v}_3, \bar{\mathbf{v}}_3] = \begin{bmatrix} 1 & 1 & 1 & 1 \\ 1 & 1 & -1 & -1 \\ \lambda_1 & \bar{\lambda}_1 & \lambda_3 & \bar{\lambda}_3 \\ \lambda_1 & \bar{\lambda}_1 & -\lambda_3 & -\bar{\lambda}_3 \end{bmatrix}. \quad (56)$$

We can rewrite equation (55) in the form of (22)

$$\dot{\mathbf{q}} = \text{diag}(\lambda_1, \bar{\lambda}_1, \lambda_3, \bar{\lambda}_3)\mathbf{q} + \mathbf{T}^{-1}\mathbf{F}(\mathbf{T}\mathbf{q}) = \mathbf{\Lambda}\mathbf{q} + \mathbf{G}(\mathbf{q}). \quad (57)$$

To compute $\mathbf{W}(\mathcal{E}_2)$, equation (55) must be diagonalized via a similar linear change of coordinates $\mathbf{x} = \tilde{\mathbf{T}}\tilde{\mathbf{q}}$, where the columns of $\tilde{\mathbf{T}}$ now contain the eigenvectors of (55) in the following order

$$\tilde{\mathbf{T}} = [\mathbf{v}_3, \bar{\mathbf{v}}_3, \mathbf{v}_1, \bar{\mathbf{v}}_1] = \begin{bmatrix} 1 & 1 & 1 & 1 \\ -1 & -1 & 1 & 1 \\ \lambda_3 & \bar{\lambda}_3 & \lambda_1 & \bar{\lambda}_1 \\ -\lambda_3 & -\bar{\lambda}_3 & \lambda_1 & \bar{\lambda}_1 \end{bmatrix}. \quad (58)$$

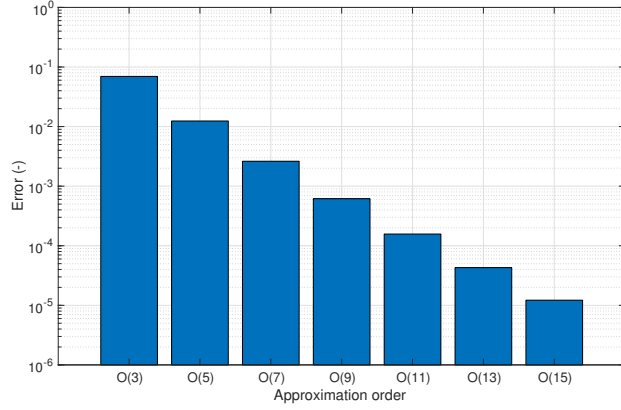
Similarly, equation (55) can be written in the form of (22), i.e.

$$\dot{\tilde{\mathbf{q}}} = \text{diag}(\lambda_3, \bar{\lambda}_3, \lambda_1, \bar{\lambda}_1)\tilde{\mathbf{q}} + \tilde{\mathbf{T}}^{-1}\mathbf{F}(\tilde{\mathbf{T}}\tilde{\mathbf{q}}) = \tilde{\mathbf{\Lambda}}\tilde{\mathbf{q}} + \tilde{\mathbf{G}}(\tilde{\mathbf{q}}). \quad (59)$$

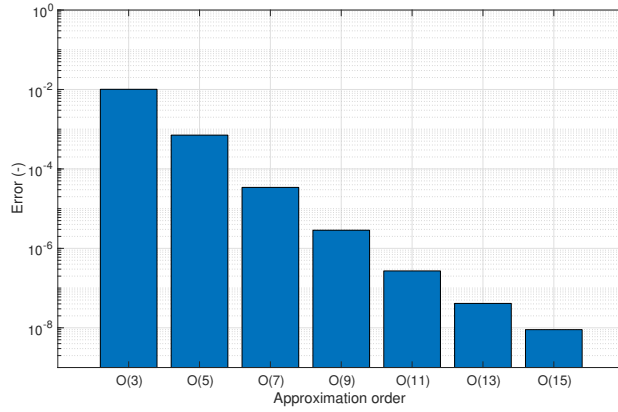
The polynomial expressions for the nonlinearities $\mathbf{G}(\mathbf{q})$ and $\tilde{\mathbf{G}}(\tilde{\mathbf{q}})$ only contain cubic nonlinearities and therefore only the nonlinear coefficient matrices \mathbf{G}_3 and $\tilde{\mathbf{G}}_3$ will be non-zero. We will compute $\mathbf{W}(\mathcal{E}_1)$ and $\mathbf{W}(\mathcal{E}_2)$ for the following parameter values

$$k = 1 \text{ N m}^{-1}, \quad c = 0.03 \text{ N s m}^{-1}, \quad \kappa = 0.5 \text{ N m}^{-3}, \quad \delta = 0.05. \quad (60)$$

We justify the choice up to which order we have to approximate the SSMS to get an accurate reduced order model, by evaluating the invariance error (50) for different approximation orders. For a given fixed radius $\rho_0 = 0.35$ we take 50 initial points, each corresponding to an angle θ_0 , uniformly distributed in S^1 .



(a)



(b)

Figure 5: Normalized error for the 3th-15th order approximation of $\mathbf{W}(\mathcal{E}_1)$ (5a) and $\mathbf{W}(\mathcal{E}_2)$ (5b) for 50 evenly distributed initial positions lying on a fixed radius $\rho_0 = 0.35$ and $\theta_0 \in S^1$. For each trajectory traveling between ρ_0 and $\rho_\epsilon = 0.01$, we identify the maximum error and take the average over all trajectories.

As the order of the approximation of $\mathbf{W}(\mathcal{E}_1)$ and $\mathbf{W}(\mathcal{E}_2)$ is increased, the error δ_{inv} is substantially reduced, as expected. We conclude that the 15th order approximation for both spectral submanifolds is high enough to guarantee them to be accurate for oscillation amplitudes up to $\rho_0 = 0.35$, which corresponds to a physical maximum displacement of $|x_1| \approx 0.66$ m and $|x_2| \approx 0.71$ m for $\mathbf{W}(\mathcal{E}_1)$ and $|x_1| \approx 0.73$ m and $|x_2| \approx 0.66$ m for $\mathbf{W}(\mathcal{E}_2)$.

We observe that the following near-inner-resonances conditions are satisfied within the spectral subspaces \mathcal{E}_1 and \mathcal{E}_2 , see table (1a) and (1b) respectively.

\mathcal{E}_1					\mathcal{E}_2				
	a	b	λ_l	I		a	b	λ_l	I
$\mathcal{O}(\mathbf{z} ^3)$	2	1	λ_1	0.00707	$\mathcal{O}(\mathbf{z} ^3)$	2	1	λ_3	0.01225
	1	2	$\bar{\lambda}_1$	0.00707		1	2	$\bar{\lambda}_3$	0.01225
$\mathcal{O}(\mathbf{z} ^5)$	3	2	λ_1	0.00926	$\mathcal{O}(\mathbf{z} ^5)$	3	2	λ_3	0.01604
	2	3	$\bar{\lambda}_1$	0.00926		2	3	$\bar{\lambda}_3$	0.01604
$\mathcal{O}(\mathbf{z} ^7)$	4	3	λ_1	0.01019	$\mathcal{O}(\mathbf{z} ^7)$	4	3	λ_3	0.01765
	3	4	$\bar{\lambda}_1$	0.01019		3	4	$\bar{\lambda}_3$	0.01765
$\mathcal{O}(\mathbf{z} ^9)$	5	4	λ_1	0.01069	$\mathcal{O}(\mathbf{z} ^9)$	5	4	λ_3	0.01852
	4	5	$\bar{\lambda}_1$	0.01069		4	5	$\bar{\lambda}_3$	0.01852
$\mathcal{O}(\mathbf{z} ^{11})$	6	5	λ_1	0.01100	$\mathcal{O}(\mathbf{z} ^{11})$	6	5	λ_3	0.01905
	5	6	$\bar{\lambda}_1$	0.01100		5	6	$\bar{\lambda}_3$	0.01905
$\mathcal{O}(\mathbf{z} ^{13})$	7	6	λ_1	0.01121	$\mathcal{O}(\mathbf{z} ^{13})$	7	6	λ_3	0.01941
	6	7	$\bar{\lambda}_1$	0.01121		6	7	$\bar{\lambda}_3$	0.01941
$\mathcal{O}(\mathbf{z} ^{15})$	8	7	λ_1	0.01136	$\mathcal{O}(\mathbf{z} ^{15})$	8	7	λ_3	0.01967
	7	8	$\bar{\lambda}_1$	0.01136		7	8	$\bar{\lambda}_3$	0.01967

(a)
(b)

Table 1: Near-inner-resonances for \mathcal{E}_1 and \mathcal{E}_2 with $\delta = 0.05$.

We intend to remove the near-inner resonant terms $z_1^2 z_2$, $z_1 z_2^2$, $z_1^3 z_2^2$, $z_1^2 z_2^3$, $z_1^4 z_2^3$, $z_1^3 z_2^4$, $z_1^5 z_2^4$, $z_1^4 z_2^5$, $z_1^6 z_2^5$, $z_1^5 z_2^6$, $z_1^7 z_2^6$, $z_1^6 z_2^7$, $z_1^8 z_2^7$ and $z_1^7 z_2^8$ in the expressions of $\mathbf{W}(\mathcal{E}_1)$ and $\mathbf{W}(\mathcal{E}_2)$ and add them to the polynomial expressions for the reduced dynamics on the spectral submanifolds. Due to the choice of nonlinearities, all the coefficients of $\mathbf{W}(\mathcal{E}_1)$ and $\mathbf{W}(\mathcal{E}_2)$ corresponding to even powers in $|\mathbf{z}|$ are zero. Solving the partitioned Sylvester equations (33) and (34) for $\mathbf{W}_i^{\mathcal{E}}$ and $\mathbf{W}_i^{\mathcal{C}}$ for orders $i = 2, \dots, 15$, we obtain the lower-dimensional projections of the full phase space for the 15th order approximations of $\mathbf{W}(\mathcal{E}_1)$ and $\mathbf{W}(\mathcal{E}_2)$, shown in figure 6. The images are directly obtained from SSMtool, which detects resonant terms and adds them to the reduced dynamics $\mathbf{R}(\mathbf{z})$ when solving the partitioned Sylvester equations (33) and (34).

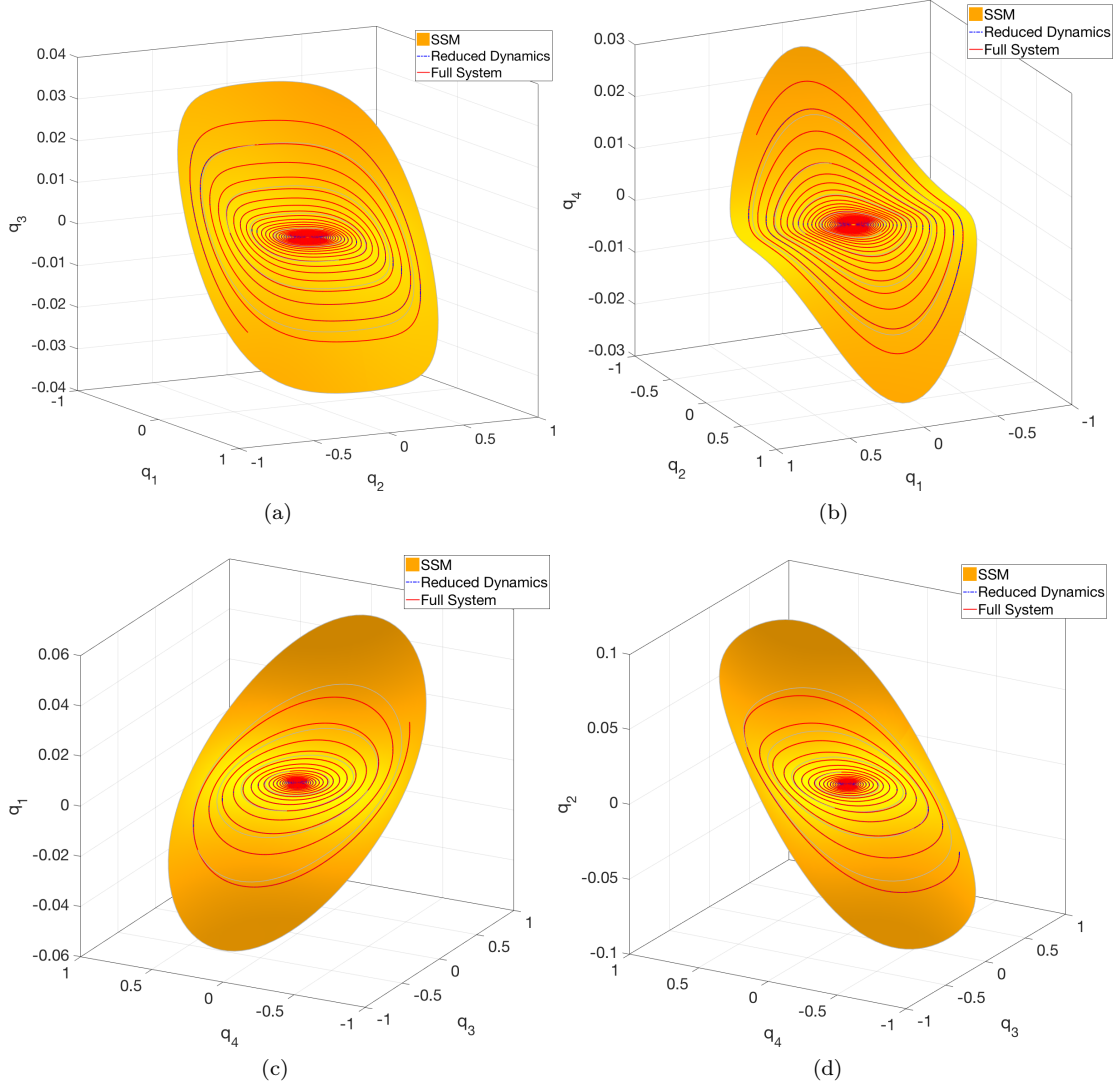


Figure 6: Lower-dimensional projections of the full phase space, showing the 15th order approximations of $\mathbf{W}(\mathcal{E}_1)$ and $\mathbf{W}(\mathcal{E}_2)$. Figures 6a and 6b show the spectral submanifold $\mathbf{W}(\mathcal{E}_1)$ tangent to \mathcal{E}_1 . Figures 6c and 6d show the spectral submanifold $\mathbf{W}(\mathcal{E}_2)$ tangent to \mathcal{E}_2 . The dashed curves indicate different projections of a trajectory of the reduced system $\mathbf{R}(\mathbf{z})$, starting from the initial position $\rho = 0.35$ and $\theta = 1$. The solid curves represent trajectories of the full system for the same initial position. The solid gray curves represent contour lines of equal parameterized distance ρ .

7.1.2. Reduced Dynamics

The near-inner resonances within the spectral subspaces \mathcal{E}_1 and \mathcal{E}_2 introduce nonlinear terms in the reduced dynamics on the spectral submanifolds. The reduced dynamics on $\mathbf{W}(\mathcal{E}_1)$ and $\mathbf{W}(\mathcal{E}_2)$ is of the general form (45). After transforming to polar coordinates, we obtain the following reduced equations for the in-phase mode of the system from SSMtool:

$$\dot{\rho} = -0.015\rho - 0.00079121\rho^5 - 0.0012708\rho^7 \quad (61)$$

$$+ 0.0090446\rho^9 - 0.03569\rho^{11} + 0.12918\rho^{13} - 0.45878\rho^{15}, \quad (62)$$

$$\omega = 0.99989 + 0.37504\rho^2 - 0.60592\rho^4 + 1.1713\rho^6$$

$$- 2.5137\rho^8 + 5.7885\rho^{10} - 14.01\rho^{12} + 35.159\rho^{14}.$$

The reduced dynamics for the out-of-phase mode of the system is obtained from SSMtool as

$$\dot{\rho} = -0.045\rho + 0.016267\rho^5 + 0.02614\rho^7 \quad (63)$$

$$+ 0.015714\rho^9 - 0.012768\rho^{11} - 0.03437\rho^{13} - 0.0308\rho^{15},$$

$$\omega = 1.7315 + 0.21658\rho^2 + 0.19904\rho^4 + 0.14858\rho^6 \quad (64)$$

$$+ 0.072849\rho^8 + 0.017657\rho^{10} + 0.004087\rho^{12} - 0.011824\rho^{14},$$

where we set the order of computations to $\mathcal{O}(15)$. Both instantaneous frequencies (62) and (64) depend on ρ only. The two red curves in figure 7a and figure 7b represent the $\mathcal{O}(15)$ backbone curves for the in-phase and out-of-phase mode of the mechanical system, whereas the blue curves display the $\mathcal{O}(3)$ approximations of the backbone curves.

We used the numerical continuation software COCO [25] to find periodic orbits of the periodically forced system for a fixed forcing amplitude while varying the forcing frequency. We have extensively optimized the continuation parameters to ensure accurate but fast results. In the current work, COCO is used as an off-the-shelf open-source benchmark to which we compare SSMtool as a stand-alone package. The promising techniques of Blanc et al. [13] and Renson et al. [15] would be expected to perform better than COCO in these computations, but have no available open-source implementations at this point.

The equations of motion of the forced system are

$$\begin{bmatrix} m & 0 \\ 0 & m \end{bmatrix} \begin{bmatrix} \ddot{x}_1 \\ \ddot{x}_2 \end{bmatrix} + \begin{bmatrix} 2c & -c \\ -c & 2c \end{bmatrix} \begin{bmatrix} \dot{x}_1 \\ \dot{x}_2 \end{bmatrix} + \begin{bmatrix} 2k & -k \\ -k & 2k \end{bmatrix} \begin{bmatrix} x_1 \\ x_2 \end{bmatrix} + \begin{bmatrix} \kappa x_1^3 \\ 0 \end{bmatrix} = \begin{bmatrix} A \cos \omega t \\ 0 \end{bmatrix}, \quad (65)$$

where we use the same parameter values (60) and introduced a forcing term with amplitude A and forcing frequency ω . The resulting periodic response amplitudes are shown in figure 7a and figure 7b in black for a forcing amplitude of $A = 0.05$ N and $A = 0.2$ N, respectively. As shown, the $\mathcal{O}(15)$ approximations for both backbone curves fit the forced peak responses well. The computational time for the continuation curve in figure 7a takes 8 minutes and 6 seconds on a Mac Pro 2×3.06 GHz 6-Core Intel Xeon, which technically corresponds to a single point on the backbone curve. The computational time for the backbone curve, extracted from the 15th order approximation of $\mathbf{W}(\mathcal{E}_1)$, is approximately 3 minutes, resulting in a parameterized curve that can be subsequently evaluated at any required frequency. The computational time for the continuation curve in figure 7b takes a total of 11 minutes and 16 seconds, whereas the computational time for the backbone curve, extracted from the 15th order approximation of $\mathbf{W}(\mathcal{E}_2)$, is also approximately 3 minutes.

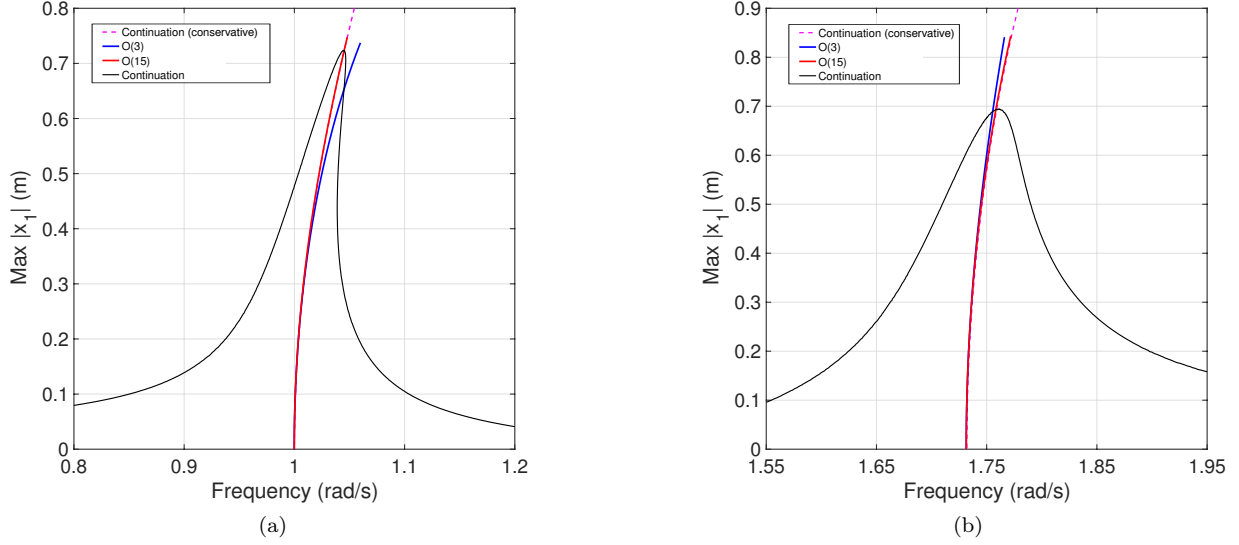


Figure 7: Backbone curves and periodically forced responses for different amplitudes of the mechanical system (51). Figure 7a shows the $\mathcal{O}(15)$ (red) and $\mathcal{O}(3)$ (blue) approximations of the backbone curves for the in-phase mode of the system. Figure 7b shows the $\mathcal{O}(15)$ (red) and $\mathcal{O}(3)$ (blue) approximations of the backbone curves for the out-of-phase mode of the system. Black lines mark amplitudes of periodic orbits of the periodically forced system for different forcing amplitudes for varying forcing frequency. The dashed lines (magenta) represent the backbone curves extracted from COCO in the conservative limit of the mechanical system, without any forcing.

7.2. The modified Shaw–Pierre example: Outer resonances

We now consider the same analytic example as in section 7.1, but with the linear springs k_1 , k_2 , k_3 and the damping c tuned such that there are near-outer resonances and no near-inner resonances. Here we only compute $\mathbf{W}(\mathcal{E}_1)$, the slow SSM arising from the slow complex pair of eigenvalues. By definition, it is impossible to obtain an outer resonance for the spectral subspace corresponding to the remaining fast complex pair of eigenvalues.

The current example is taken from work of Cirillo et al. [26], where a global parameterization method is proposed for the computation of invariant manifolds in a domain where the stringent non-resonance conditions of analytic linearization hold.

For the parameter values

$$k_1 = k_3 = 1 \text{ N m}^{-1}, \quad k_2 = 4.005 \text{ N m}^{-1}, \quad c = 0.4 \text{ N s m}^{-1}, \quad \kappa = 0.5 \text{ N m}^{-3}, \quad \delta = 0.05, \quad (66)$$

the system has two complex conjugate pairs of eigenvalues with

$$\begin{aligned} \lambda_1 &= -0.2 + 0.9798i, \\ \lambda_2 &= -0.6 + 2.9411i, \end{aligned}$$

and their conjugates. We construct the two-dimensional spectral subspace \mathcal{E}_1 corresponding to the first conjugate pair of slow eigenvalues λ_1 and $\bar{\lambda}_1$, whose inner and outer spectral quotients are

$$\sigma_{\text{in}}(\mathcal{E}_1) = \text{Int} \begin{bmatrix} \text{Re}\lambda_1 \\ \text{Re}\lambda_1 \end{bmatrix} = 1. \quad (67)$$

$$\sigma_{\text{out}}(\mathcal{E}_1) = \text{Int} \begin{bmatrix} \text{Re}\bar{\lambda}_2 \\ \text{Re}\lambda_1 \end{bmatrix} = 3, \quad (68)$$

The exact inner and outer non-resonance conditions, (9) and (13) respectively, again are satisfied for the spectral subspace \mathcal{E}_1 , i.e., there exists a two-dimensional analytic SSMs, $\mathbf{W}(\mathcal{E}_1)$, that is unique among all C^4 invariant manifolds tangent to \mathcal{E}_1 . Due to the higher choice of damping, there are no near-inner resonances and hence the reduced dynamics on the manifold can be expressed as linear. However, the SSM is close to having two third-order outer resonances which in turn leads to the two near-outer resonances shown in table 2. For $k_2 = 4 \text{ N m}^{-1}$, the SSM construction will break down as Θ_3^c becomes singular while equation (34) has a nonzero right-hand side.

\mathcal{E}_1				
	a	b	λ_l	I
$\mathcal{O}(\mathbf{z} ^3)$	3	0	λ_2	0.000162
	0	3	$\bar{\lambda}_2$	0.000162

Table 2: Near-outer-resonances for \mathcal{E}_1 with $\delta = 0.05$.

As has been done in section 7.1.1, we would like to identify the order to which we have to approximate the SSM to obtain an accurate reduced order model. Using the invariance measure defined in equation (50), we test the invariance of $\mathbf{W}(\mathcal{E}_1)$ for different approximation orders. In figure 8, we show the invariance error for seven different approximations of $\mathbf{W}(\mathcal{E}_1)$. For a given fixed radius $\rho_0 = 0.28$ we take 50 initial points, each corresponding to an angle θ_0 , uniformly distributed in S^1 .

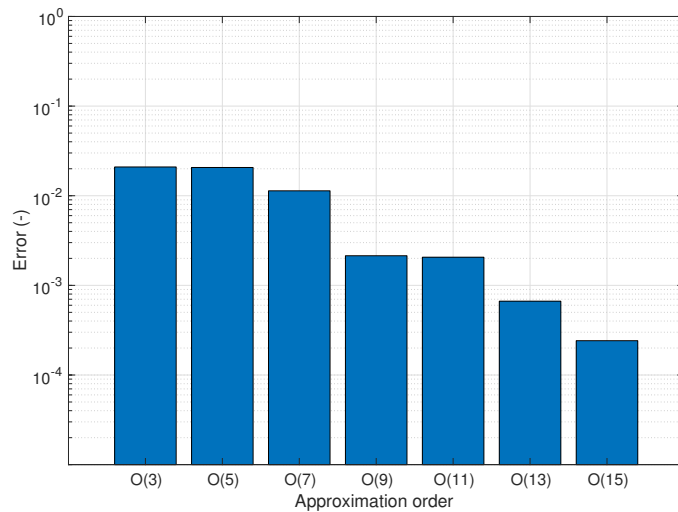


Figure 8: Invariance error for the 3th-15th order approximations of $\mathbf{W}(\mathcal{E}_1)$ for 50 evenly distributed initial positions lying on a fixed radius $\rho_0 = 0.28$ and $\theta_0 \in S^1$. For each trajectory traveling between ρ_0 and $\rho_\epsilon = 0.01$, we identify the maximum error and take the average over all trajectories.

As the SSM is near an outer resonance, a folding of the SSM over its underlying modal subspace is more likely to occur. Such a folding is illustrated in figure 9, showing a lower-dimensional projection of the full phase space of the 15th order approximation of $\mathbf{W}(\mathcal{E}_1)$. This example brings out the power of the parameterization method, as constructing the SSM as a graph over its modal subspace would break down at the point of folding.

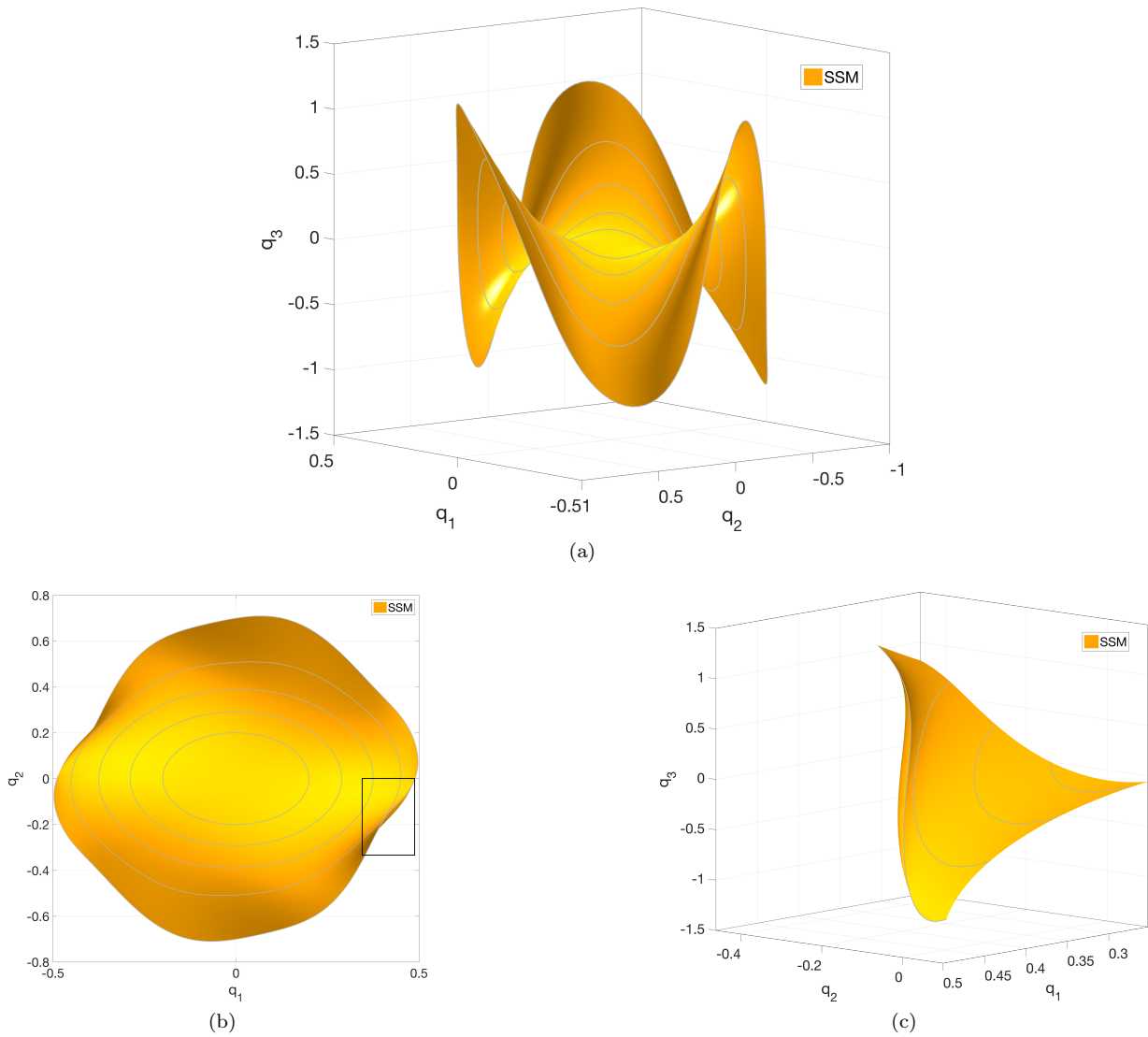


Figure 9: Lower-dimensional projections of the full phase space showing the 15th order approximation of $\mathbf{W}(\mathcal{E}_1)$ in modal coordinates. Figures 9a, 9b and 9c show the spectral submanifold $\mathbf{W}(\mathcal{E}_1)$ tangent to \mathcal{E}_1 , being close to outer resonance. Figure 9b, a top-view of $\mathbf{W}(\mathcal{E}_1)$, shows the development of a fold as indicated by the rectangle. Figure 9c is a zoomed-in version of the fold.

In figure 10, we show the SSM transformed to physical coordinates (also an option in SSMtool), where we demonstrate the invariance of $\mathbf{W}(\mathcal{E}_1)$ (figure 10a) and that different trajectories converge towards $\mathbf{W}(\mathcal{E}_1)$ (figure 10b), when starting close to $\mathbf{W}(\mathcal{E}_1)$.

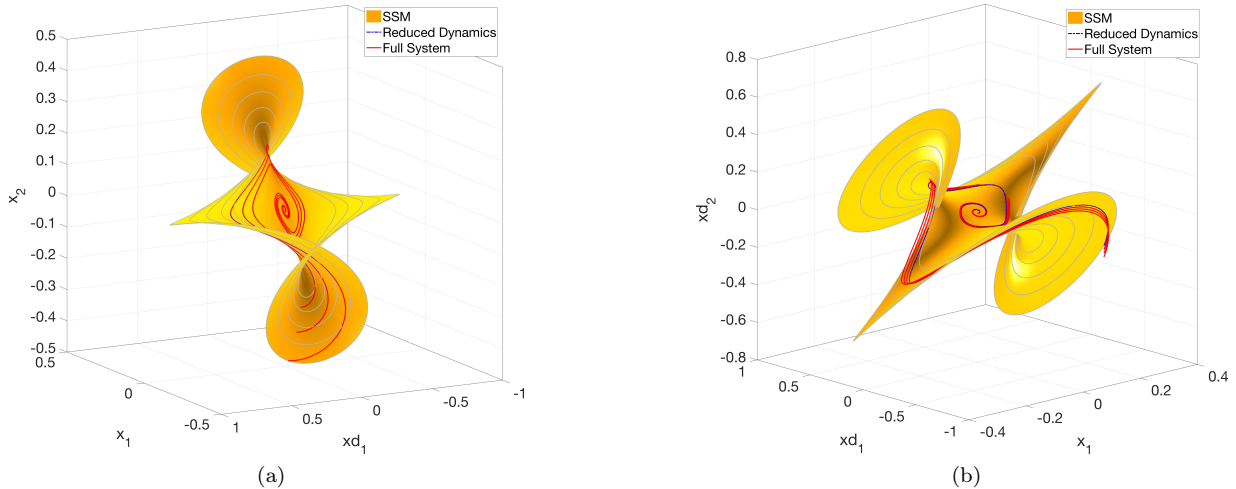


Figure 10: Lower-dimensional projections of the full phase space showing the 15th order approximation of $\mathbf{W}(\mathcal{E}_1)$, transformed to physical coordinates. The dashed curves in figure 10a correspond to trajectories of the reduced system $\mathbf{R}(\mathbf{z})$ corresponding to the initial positions $\rho = \{0.15, 0.13, 0.11\}$ and $\theta = 3$. The solid curves represent trajectories of the full system for the same initial positions. In figure 10b, the dashed curves corresponds to a trajectory of the reduced system $\mathbf{R}(\mathbf{z})$ for the initial position $\rho = 0.15$ and $\theta = 1$. The solid lines represent trajectories of the full system having an initial position off the manifold, showing the convergence towards $\mathbf{W}(\mathcal{E}_1)$.

7.3. The discretized nonlinear Timoshenko beam

In this section, we construct a reduced order model for a discretized nonlinear Timoshenko beam by computing the reduced dynamics on the two-dimensional SSM arising from the slowest modal subspace. We will briefly outline the steps leading to the derivation of the partial differential equations (PDEs) governing the dynamics of the beam. Our reasoning largely follows the presentation given by Reddy [27]. The problem considered here is a square 2D beam placed in a cartesian coordinate system with coordinates (x, y, z) and basis $(\mathbf{e}_x, \mathbf{e}_y, \mathbf{e}_z)$. Initially, the beam is straight, with its main axis parallel to the x -axis, while its cross section lies in the $y - z$ plane. The relevant beam parameters are listed in table 3.

Symbol	Meaning (unit)
L	Length of beam (mm)
h	Height of beam (mm)
b	Width of beam (mm)
ρ	Density (kg mm^{-3})
E	Young's Modulus (MPa)
G	Shear Modulus (MPa)
η	Axial material damping constant (MPa s)
μ	Shear material damping constant (MPa s)
λ	External damping constant (MPa s mm^{-2})
$A = bh$	Cross-section of beam (mm^2)

Table 3: Notation used in subsequent derivations

We call the line that initially coincides with the x -axis the beam's neutral axis. The kinematic assumptions underlying the Timoshenko beam model can be obtained by relaxing the restrictions of the Bernoulli hypothesis which is the basis of the more classical and well-known Euler-Bernoulli beam theory. The Bernoulli hypothesis states (cf. Reddy [27]) that initially straight material lines normal to the neutral axis remain (a) straight and (b) inextensible after deformation, and (c) rotate as rigid lines to remain per-

pendicular to the beam's neutral axis after deformation. We relax (c) by allowing for rigid rotation of the cross section about the y -axis. These kinematic assumptions are satisfied by the following displacement field

$$u_x(x, y, z) = u_0(x) + z\phi_y(x), \quad (69)$$

$$u_y(x, y, z) = 0, \quad (70)$$

$$u_z(x, y, z) = w(x). \quad (71)$$

Here (u_x, u_y, u_z) are the components of the displacement field $\mathbf{u}(x, y, z)$ for a material point in the (x, y, z) directions, respectively. The functions $u_0(x)$ and $w(x)$ represent the displacements of a material point with initial coordinates on the beam's neutral axis, given by $z = 0$. The rotation of a normal section about the y -axis is denoted by $\phi_y(x)$. We illustrate the kinematics in figure 11.

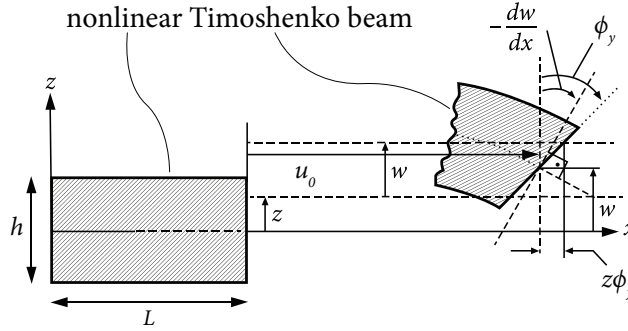


Figure 11: Kinematics of the nonlinear Timoshenko beam.

Following Reddy [27], we neglect all $(u_{0,x})^2$ terms in the Green-Lagrange strain tensor, where we use the shorthand notation $(\cdot)_{,x} = \partial_x(\cdot)$. This approximation accounts for geometric nonlinearities due to moderately large rotations while assuming small membrane strains. The relevant non-zero components of the simplified Green-Lagrange strain tensor ε_{ij} take the form

$$\varepsilon_{xx} = \varepsilon_{xx}^0 + z\varepsilon_{xx}^1, \quad (72)$$

$$\gamma_{xz} = 2\varepsilon_{xy} = \gamma_{xz}^0 + z\gamma_{xz}^1, \quad (73)$$

with

$$\varepsilon_{xx}^0 = \partial_x u_0 + \frac{1}{2}(\partial_x w)^2, \quad \varepsilon_{xx}^1 = \partial_x \phi_y, \quad (74)$$

$$\gamma_{xz}^0 = \phi_y + \partial_x w + \phi_y \partial_x u_0, \quad \gamma_{xz}^1 = \phi_y \partial_x \phi_y. \quad (75)$$

We assume a linear viscoelastic constitutive relation between the stresses and strains of the following form

$$\sigma_{xx} = E\varepsilon_{xx} + \eta\dot{\varepsilon}_{xx}, \quad (76)$$

$$\sigma_{xz} = G\gamma_{xz} + \mu\dot{\gamma}_{xz}. \quad (77)$$

Here σ_{xx} and σ_{xz} are the components of the Cauchy stress tensor $\boldsymbol{\sigma}$ (see, e.g., Lai et al. [28]). The relations given in (76) and (77) are a special case of the more general linear viscoelastic material models that can be

found, for example, in Skrzypek and Ganczarski [29] and is also used, e.g., by Lesieutre and Kauffman [30]. We explain the derivation and discretization of the equations of motion of the beam in Appendix B.

In the following computations, we will consider a beam that is clamped on one end and free on the other, which means that on the clamped end all displacements (u_0, w, ϕ_y) are zero, while on the free end no restrictions are placed on the displacements. After implementation of the essential boundary conditions, the number of degrees of freedom n of our system is given by

$$n = 5m + 1, \tag{78}$$

where m is the number of finite beam elements used in the discretization. Additionally, we set the external damping parameter c , discussed in Appendix B, to zero and therefore the damping of our beam only enters through the viscoelastic constitutive relation.

We continue by constructing the slowest single-mode SSM for a specific beam, for which we will use the SSMtool to reduce the beam dynamics to a two-dimensional system of ordinary differential equations. The chosen geometric and material parameters are listed in Table 4.

Parameter	Value
L	1000 mm
h	100 mm
b	100 mm
ρ	$7850 \cdot 10^{-9} \text{ kg mm}^{-3}$
E	90 GPa
G	34.6 GPa
η	33.6 MPa s
μ	20.9 MPa s

Table 4: Geometric and material parameters.

We simulate the beam with three elements, resulting in a 32-dimensional phase space. For the chosen parameter values, the eigenvalues corresponding to the slowest modal subspace \mathcal{E} are $\lambda_{1,2} = -0.02286 \pm 11.03i$. In terms of its exponential decay rate, the eigenspace \mathcal{E} is about 50 times slower compared to the second slowest eigenspace of the system. This spectral ratio indicates that trajectories of the system transverse to the slow SSM die out fast, making the slowest SSM an excellent choice for model reduction, because it will contain trajectories that remain active for the longest time.

In figure 12, we show the invariance error (50) for four different orders of approximations of $\mathbf{W}(\mathcal{E})$.

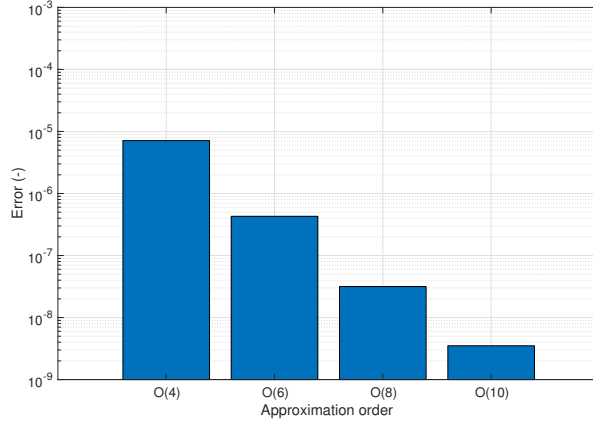


Figure 12: Invariance error for the 4th, 6th, 8th and 10th order approximations of $\mathbf{W}(\mathcal{E})$ for 50 evenly distributed initial positions lying on a fixed radius $\rho_0 = 1.5$ and $\theta_0 \in S^1$. The chosen value of $\rho_0 = 1.5$ corresponds to a maximum physical vertical displacement of the endpoint of the beam of 160 mm. For each trajectory traveling between ρ_0 and $\rho_\epsilon = 0.2$, we identify the maximum error and take the average over all trajectories.

We observe that the 4th order approximation of $\mathbf{W}(\mathcal{E})$ is already accurate up to the chosen value of $\rho_0 = 1.5$, which corresponds to a maximum physical vertical displacement of the endpoint of the beam of 160 mm. By increasing the order of approximation to 10, the invariance error is reduced further by approximately three orders of magnitude. Figure 13 displays two lower-dimensional projections of the 32-dimensional phase space, showing the 10th order approximation of $\mathbf{W}(\mathcal{E})$, with the modal coordinates q_3 and q_4 plotted over the coordinates q_1 and q_2 .

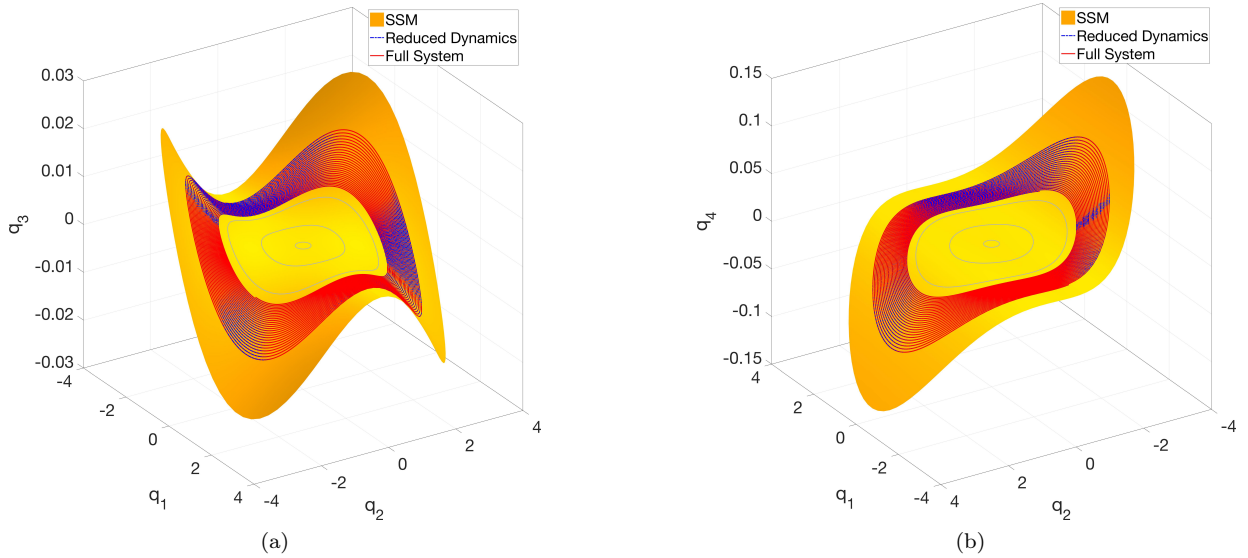


Figure 13: Lower-dimensional projections of the 32-dimensional phase space, of the discretized nonlinear Timoshenko beam, showing the 10th order approximation of $\mathbf{W}(\mathcal{E})$. Figures 13a, 13b show the spectral submanifold $\mathbf{W}(\mathcal{E})$ tangent to slowest modal subspace \mathcal{E} . The dashed curve corresponds to a trajectory of the reduced two-dimensional system $\mathbf{R}(z)$ corresponding to the initial positions $r = 1.5$ and $\theta = 3$. The solid curve represents a trajectory of the full system for the same initial position, with $t_{\text{end}} = 15$ s.

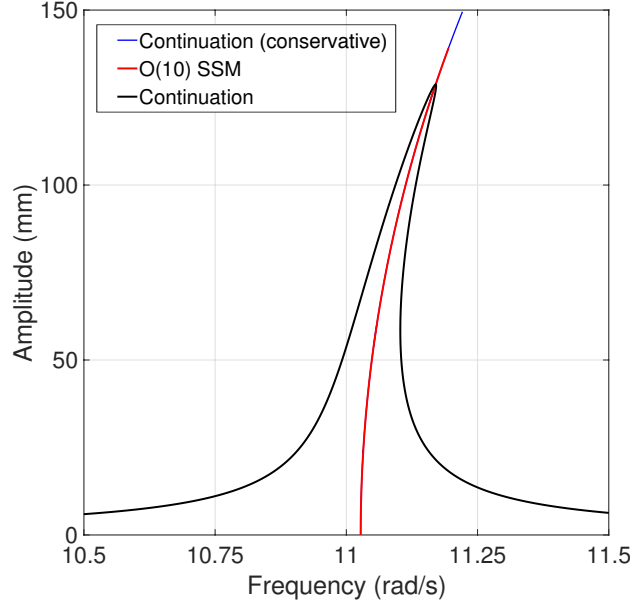


Figure 14: Backbone curve and periodically forced responses of the discretized Timoshenko beam having a 32-dimensional phase space. The $\mathcal{O}(10)$ (red) approximation of the backbone curve is computed up to $\rho = 1.3$. The black line corresponds to periodic orbits of the periodically forced system for varying forcing frequency. The blue line represents the backbone curve extracted from COCO in the conservative limit of the beam, without any forcing.

As λ_1 and $\bar{\lambda}_1$ have small negative real parts, the near-inner-resonances conditions related to $\mathcal{O}(|\mathbf{z}|^i)$ with $i = 3, 5, 7, 9$ are satisfied within the spectral subspaces \mathcal{E} . This in turn leads to the following expressions for reduced dynamics on $\mathbf{W}(\mathcal{E})$, obtained from SSMtool:

$$\begin{aligned} \dot{\rho} = & -0.022856\rho - 0.00017033\rho^3 - 4.9542 \cdot 10^{-6}\rho^5 \\ & + 8.5365 \cdot 10^{-8}\rho^7 - 3.0348 \cdot 10^{-9}\rho^9, \end{aligned} \quad (79)$$

$$\begin{aligned} \omega = & 11.027 + 0.099097\rho^2 - 0.000020843\rho^4 - 2.8625 \cdot 10^{-6}\rho^6 \\ & + 1.729 \cdot 10^{-7}\rho^8 \end{aligned} \quad (80)$$

Using the definition of the instantaneous amplitude (48) and the corresponding instantaneous frequency (80), SSMtool computes the parameterized backbone curve \mathcal{B} (shown in figure 14) in less than 4 minutes time. The continuation curve, shown in black, has been computed using the numerical continuation software COCO [25], after applying a periodic force, $F = A \cos \omega t$, to the vertical displacement coordinate w at the free end of the beam with a forcing amplitude of $A = 300$ N.

The continuation algorithm takes 4 hours 42 minutes and 17 seconds to compute. Additionally, in figure 15 we show that trajectories starting off $\mathbf{W}(\mathcal{E}_1)$, will converge towards $\mathbf{W}(\mathcal{E}_1)$ as a consequence of having the high spectral quotient between the slowest and the remaining eigenspaces.

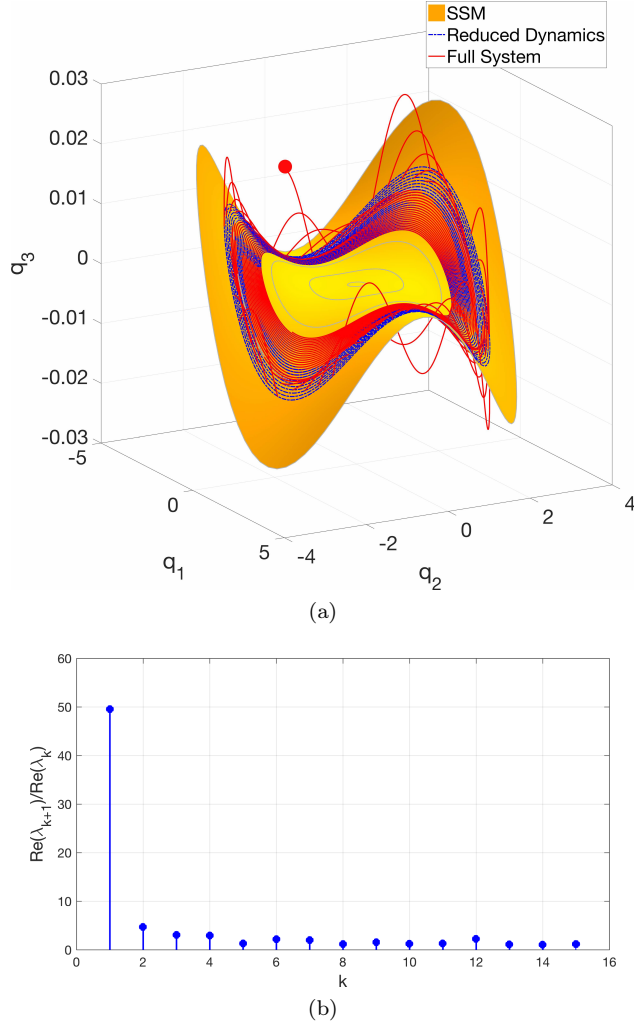


Figure 15: Lower-dimensional projections of the 32-dimensional phase space, of the discretized nonlinear Timoshenko beam, showing the 10th order approximation of $\mathbf{W}(\mathcal{E})$. Figure 15a shows the spectral submanifold $\mathbf{W}(\mathcal{E})$ tangent to slowest subspace \mathcal{E} . The dashed (blue) curve corresponds to a trajectory of the reduced two-dimensional system $\mathbf{R}(\mathbf{z})$ corresponding to the initial positions $r = 1.5$ and $\theta = 3$. The solid (red) curve represents a trajectory of the full system having an initial position off the manifold, showing the convergence towards $\mathbf{W}(\mathcal{E}_1)$, with $t_{\text{end}} = 15$ s. The collapsing nature of the trajectories onto $\mathbf{W}(\mathcal{E})$, is a direct consequence of the high spectral ratio between the slowest eigenspace and the second slowest eigenspace shown in figure 15b.

8. Future work

Currently, SSMtool is capable of computing two-dimensional spectral submanifolds in autonomous non-linear mechanical systems of arbitrary degrees of freedom. As future work, we can extend the current setting to higher-dimensional spectral submanifolds and, additionally, allow for possible forcing, as the underlying theory is already worked out in Haller and Ponsioen [9].

9. Conclusions

We have developed and tested an automated computational algorithm for two-dimensional autonomous SSMs that extends modal subspaces of linear systems to nonlinear systems. Implemented in the MATLAB

package SSMtool, the algorithm can handle non-conservative mechanical systems of arbitrary (finite) degrees of freedom, subject to numerical memory limitations only. We used a systematic approach, the parameterization method, allowing us to construct the SSMs, their reduced dynamics and corresponding backbone curves up to any required order of precision.

Because the SSMs are embedded using the parameterization method, the construction of the SSMs does not break down when the SSM folds over its underlying spectral subspace, as opposed to constructing the SSMs as graphs over a set of coordinates. The implementation (a MATLAB based graphical user interface called SSMtool) detects near-outer and near-inner resonances. In case of an exact outer resonance, the SSM construction will break down, whereas the presence of near-inner resonances in general leads to nonlinear terms in the reduced dynamics on the SSMs.

Szalai et al. [10] have exactly shown how backbone curves can be extracted from SSMs. We computed the backbone curves, in this fashion, up to 15th-order for a two-degree-of-freedom non-conservative mechanical system and used the numerical continuation software COCO [25] to find periodic orbits of the periodically forced system for different forcing amplitudes while varying the forcing frequency to verify the accuracy of the backbone curves.

Under an approximate outer resonance, folding of the SSMs is likely to occur. We demonstrated such folding on the same two-degree-of-freedom non-conservative mechanical system by varying the system parameters accordingly to create a near-outer resonance.

Finally, we have used the developed numerical method to construct a reduced-order model for a discretized nonlinear Timoshenko beam. We have computed the reduced dynamics on the two-dimensional slow SSM arising from the slowest modal subspace of the linearized system. The backbone curve obtained from the SSMtool shows close agreement with a single amplitude frequency sweep computed from COCO. While substantially limited in its scope relative to COCO's, SSMtool has returned backbone curves in a fraction of the times required by COCO to construct the response curve for one forcing amplitude. The spectral quotient between the slowest eigenspace and the second slowest eigenspace indicates that trajectories transverse to the slow SSM die out fast, making the slowest SSM an optimal choice for reducing our beam model to a two-dimensional system of ordinary differential equations.

Acknowledgments

We are grateful to Hinke Osinga and Harry Dankowicz for useful remarks and technical explanations on the numerical continuation toolbox COCO [25]. We are also thankful to Shobhit Jain, Thomas Breunung and Zsolt Verasztó for helpful discussions.

Appendix A. Properties of the Kronecker product

In this section, we list several useful properties of the Kronecker product. For further reading, we refer the reader to A.J. Laub [22].

(i) The Kronecker product is associative, i.e.,

$$\begin{aligned} (\mathbf{A} \otimes \mathbf{B}) \otimes \mathbf{C} &= \mathbf{A} \otimes (\mathbf{B} \otimes \mathbf{C}), \\ \mathbf{A} \in \mathbb{C}^{m \times n}, \quad \mathbf{B} \in \mathbb{C}^{p \times q}, \quad \mathbf{C} \in \mathbb{C}^{r \times s}. \end{aligned} \tag{A.1}$$

(ii) The Kronecker product is right-distributive, i.e.,

$$\begin{aligned} (\mathbf{A} + \mathbf{B}) \otimes \mathbf{C} &= \mathbf{A} \otimes \mathbf{C} + \mathbf{B} \otimes \mathbf{C}, \\ \mathbf{A}, \mathbf{B} \in \mathbb{C}^{m \times n}, \quad \mathbf{C} \in \mathbb{C}^{p \times q}. \end{aligned} \tag{A.2}$$

(iii) The Kronecker product is left-distributive, i.e.,

$$\begin{aligned} \mathbf{A} \otimes (\mathbf{B} + \mathbf{C}) &= \mathbf{A} \otimes \mathbf{B} + \mathbf{A} \otimes \mathbf{C}, \\ \mathbf{A} \in \mathbb{C}^{m \times n}, \quad \mathbf{B}, \mathbf{C} &\in \mathbb{C}^{p \times q}. \end{aligned} \quad (\text{A.3})$$

(iv) The product of two Kronecker products yields another Kronecker product:

$$\begin{aligned} (\mathbf{A} \otimes \mathbf{B})(\mathbf{C} \otimes \mathbf{D}) &= \mathbf{AC} \otimes \mathbf{BD} \in \mathbb{C}^{mr \times pt}, \\ \mathbf{A} \in \mathbb{C}^{m \times n}, \quad \mathbf{B} \in \mathbb{C}^{r \times s}, \quad \mathbf{C} \in \mathbb{C}^{n \times p}, \quad \mathbf{D} \in \mathbb{C}^{s \times t}. \end{aligned} \quad (\text{A.4})$$

Appendix B. Equations of motion for the nonlinear Timoshenko beam

We derive the equations of motion for the nonlinear Timoshenko beam, based on the kinematical and constitutive assumptions made in section 7.3. Applying Hamilton's principle, we require that the true evolution of the displacement field between two specified time instances, t_1 and t_2 , is a stationary point of the action functional S . Consequently, the variation of the action functional under a virtual displacement, of our system, should be identically zero at t_1 and t_2 , i.e.,

$$\delta S = \int_{t_1}^{t_2} -\delta K + \delta U + \delta V \, dt = 0, \quad (\text{B.1})$$

where δK and δU are the variations in kinetic and strain energy due to an arbitrary virtual displacement, and δV is the virtual work done by the external forces. For simplicity, we assume that the virtual work done by internal forces acting on the beam's cross section is large relative to the work done by internal forces due to out-of-plane stresses. This corresponds to assuming a state of either plane stress or plane strain, causing all terms related to out-of-plane stresses to drop out from the expression for the internal strain energy. This assumption can be justified by the fact that the respective neglected quantities would only contribute to the governing equations nonlinear terms of the fourth order in the stiffest (and hence typically the fastest decaying) degrees of freedom, ϕ_y , while all other nonlinearities are of order three or lower. Thus, those terms can be considered small compared to the rest. This can also be shown by nondimensionalizing the system and treating the ratio of the beam's length to its height, $\frac{h}{L}$, as a small parameter.

In addition to our viscoelastic constitutive law, we allow for external damping by introducing a simple damping model similar to the ones discussed in Lesieutre and Kauffman [30] and Lesieutre [31]. Our model assumes a body force acting proportional to the displacement velocity:

$$\mathbf{f}_c = c\dot{\mathbf{u}}(x, y, z). \quad (\text{B.2})$$

The virtual work done by this force is

$$\delta V = \int_L \int_A \mathbf{f}_c \delta \mathbf{u} \, dA dx = \int_L \lambda (\dot{u}_0 \delta u_0 + \dot{w} \delta w + \frac{I_2}{I_0} \dot{\phi}_y \delta \phi_y) \, dx, \quad (\text{B.3})$$

with

$$I_k = \int_A z^k \, dA, \quad \lambda = cI_0. \quad (\text{B.4})$$

Equation (B.3) can be interpreted as the work done by two line-distributed forces, $f_x = \lambda \dot{u}_0$ and $f_z = \lambda \dot{w}$, proportional to the time derivative of the transverse displacement and the axial displacement, respectively.

Additionally, we have a line-distributed force couple, $T_y = \lambda \frac{I_2}{I_0} \dot{\phi}_y$, proportional to the time derivative of the rotation of the cross section. The pre-factor I_2/I_0 in equation (B.3) ensures that the contribution of the external damping to the damping matrix of the FEM model derived below is proportional to the mass matrix. As a consequence, the entire system will be subjected to Rayleigh damping, a damping model which is frequently used in FEM simulations, see e.g. Takács et al. [32]. For more extensive discussions about how to model damping in beams, we refer the reader to the work of Lesieutre and Kauffman [30] and Lesieutre [31]. The preceding considerations lead to the following expressions

$$\delta K = \int_L m_0 \dot{u}_0 \delta \dot{u}_0 + m_0 \dot{w} \delta \dot{w} + m_2 \dot{\phi}_y \delta \dot{\phi}_y dx, \quad (\text{B.5})$$

$$\delta U = \int_L \int_A \sigma_{xx} \delta \varepsilon_{xx} + \sigma_{xz} \delta \gamma_{xz} dA dx, \quad (\text{B.6})$$

$$\delta V = \int_L f_x \delta u_0 + f_z \delta w + T_y \delta \phi_y dx, \quad (\text{B.7})$$

with

$$m_k = \int_A \rho z^k dA, \quad (\text{B.8})$$

Substituting (B.5), (B.6) and (B.7) into (B.1), plugging in the kinematical assumptions and using integration by parts with respect to t and x we obtain

$$\begin{aligned} \delta S = & \int_{t_1}^{t_2} \int_0^L (m_0 \ddot{u}_0 + \lambda \dot{u}_0 - \partial_x (M_{xx}^0 + \phi_y M_{xz}^0)) \delta u_0 + (m_0 \ddot{w} + \lambda \dot{w} - \partial_x (M_{xz}^0 + \partial_x w M_{xx}^0)) \delta w \\ & + \left(m_2 \ddot{\phi}_y + \lambda \frac{I_2}{I_0} \dot{\phi}_y - \partial_x (M_{xx}^1 + \phi_y M_{xz}^1) + (M_{xz}^0 + \partial_x u_0 M_{xz}^0 + \partial_x \phi_y M_{xz}^1) \right) \delta \phi_y dx \\ & + [(M_{xx}^0 + \phi_y M_{xz}^0) \delta u_0]_0^L + [(M_{xz}^0 + \partial_x w M_{xx}^0) \delta w]_0^L + [(M_{xx}^1 + \phi_y M_{xz}^1) \delta \phi_y]_0^L dt = 0, \end{aligned} \quad (\text{B.9})$$

where we have defined

$$M_{ij}^k = \int_A \sigma_{ij} z^k dA. \quad (\text{B.10})$$

Equating the variational derivative of this functional with zero, we obtain the Euler-Lagrange equations

$$m_0 \ddot{u}_0 + \lambda \dot{u}_0 - \partial_x (M_{xx}^0 + \phi_y M_{xz}^0) = 0, \quad (\text{B.11})$$

$$m_0 \ddot{w} + \lambda \dot{w} - \partial_x (M_{xz}^0 + \partial_x w M_{xx}^0) = 0, \quad (\text{B.12})$$

$$m_2 \ddot{\phi}_y + \lambda \frac{I_2}{I_0} \dot{\phi}_y - \partial_x (M_{xx}^1 + \phi_y M_{xz}^1) + (M_{xz}^0 + \partial_x u_0 M_{xz}^0 + \partial_x \phi_y M_{xz}^1) = 0, \quad (\text{B.13})$$

along with the corresponding boundary conditions

$$(M_{xx}^0 + \phi_y M_{xz}^0)|_L \delta u_0(L) = 0, \quad (M_{xx}^0 + \phi_y M_{xz}^0)|_0 \delta u_0(0) = 0, \quad (\text{B.14})$$

$$(M_{xz}^0 + \partial_x w M_{xx}^0)|_L \delta w(L) = 0, \quad (M_{xz}^0 + \partial_x w M_{xx}^0)|_0 \delta w(0) = 0, \quad (\text{B.15})$$

$$(M_{xx}^1 + \phi_y M_{xz}^1)|_L \delta \phi_y(L) = 0, \quad (M_{xx}^1 + \phi_y M_{xz}^1)|_0 \delta \phi_y(0) = 0. \quad (\text{B.16})$$

The M_{ij}^k terms can be written as a function of our displacement field by using the kinematical and constitutive relations, i.e.,

$$M_{xx}^0 = I_0 \left(E(\partial_x u_0 + \frac{1}{2}(\partial_x w)^2) + \eta(\partial_x \dot{u}_0 + \partial_x \dot{w} \partial_x w) \right), \quad (\text{B.17})$$

$$M_{xx}^1 = I_2 \left(E \partial_x \phi_y + \eta \partial_x \dot{\phi}_y \right), \quad (\text{B.18})$$

$$M_{xz}^0 = I_0 \left(G(\phi_y + \partial_x w + \phi_y \partial_x u_0) + \mu(\dot{\phi}_y + \partial_x \dot{w} + \dot{\phi}_y \partial_x u_0 + \phi_y \partial_x \dot{u}_0) \right), \quad (\text{B.19})$$

$$M_{xz}^1 = I_2 \left(G \phi_y \partial_x \phi_y + \mu(\dot{\phi}_y \partial_x \phi_y + \phi_y \partial_x \dot{\phi}_y) \right). \quad (\text{B.20})$$

We discretize equations (B.11)-(B.13) using a finite-element discretization (cf. Reddy [33] for a more detailed description). We use cubic shape functions to approximate u_0 , quadratic shape functions for w and linear shape functions for ϕ_y . A beam element with three equally spaced nodes, situated at the beginning, the middle and at the end of the element is used. The node in the middle of the element is only needed for the interpolation of the transverse displacement w . To avoid shear and membrane locking, the ε_{xx}^0 and γ_{xz}^0 terms should be approximated by shape functions of the same order. After discretization, we obtain a set of n ordinary differential equations (ODEs) governing the dynamics the nonlinear Timoshenko beam:

$$\mathbf{M}\ddot{\mathbf{y}} + \mathbf{C}\dot{\mathbf{y}} + \mathbf{K}\mathbf{y} + \mathbf{f}(\mathbf{y}, \dot{\mathbf{y}}) = \mathbf{0} \quad (\text{B.21})$$

where we have defined the vector

$$\mathbf{y} = \begin{bmatrix} \tilde{u}_0 \\ \tilde{w} \\ \tilde{\phi}_y \end{bmatrix} \quad (\text{B.22})$$

representing the discretized degrees of freedom corresponding to the unknowns (u_0, w, ϕ_y) . The quantities $\mathbf{M} \in \mathbb{R}^{n \times n}$, $\mathbf{C} \in \mathbb{R}^{n \times n}$, $\mathbf{K} \in \mathbb{R}^{n \times n}$ are the mass, damping and stiffness matrices of our discretized model, respectively, and the nonlinear force vector $\mathbf{f} \in \mathbb{R}^n$ is of the form

$$f_i = D_{ijk} y_j y_k + G_{ijk} y_j \dot{y}_k + H_{ijkl} y_j y_k y_l + L_{ijkl} y_j y_k \dot{y}_l \quad (\text{B.23})$$

where $i \in \{1, \dots, n\}$, and the Einstein summation convention is followed.

Appendix C. Multiple representations for the nonlinear coefficient matrices

The vector $\mathbf{q}^{\otimes i}$ contains all possible combinations of its own elements up to order i , and therefore will contain all the monomial terms related to a homogeneous multivariate polynomial of degree i in the variables \mathbf{q} . The number of unique monomial terms $S(2n, i)$ in a multivariate polynomial of degree i with the variables $\mathbf{q} \in \mathbb{C}^{2n}$ is equal to the number of multisets of cardinality i , with elements taken from the set $\{1, 2, \dots, 2n\} \in \mathbb{N}^{2n}$ [34], i.e.,

$$S(2n, i) = \binom{i + 2n - 1}{i} = \frac{(i + 2n - 1)!}{(2n - 1)! i!}. \quad (\text{C.1})$$

To illustrate this, we now give an example.

Example 2. [Unique monomial terms representing a multivariate polynomial of degree two] Assume that $\mathbf{q} = (q_1, q_2, q_3, q_4)^T \in \mathbb{C}^4$, then the unique monomial terms related to the multivariate polynomial of degree

two in the \mathbf{q} variables are

$$\left(\begin{array}{c} q_1^2 \\ q_1 q_2 \\ q_1 q_3 \\ q_1 q_4 \\ q_2^2 \\ q_2 q_3 \\ q_2 q_4 \\ q_3^2 \\ q_3 q_4 \\ q_4 \end{array} \right) \rightarrow \left. \begin{array}{c} \{1, 1\} \\ \{1, 2\} \\ \{1, 3\} \\ \{1, 4\} \\ \{2, 2\} \\ \{2, 3\} \\ \{2, 4\} \\ \{3, 3\} \\ \{3, 4\} \\ \{4, 4\} \end{array} \right\} S = \binom{5}{2} = 10. \quad (\text{C.2})$$

Here we see the equivalence with the ten multisets of cardinality two, with elements taken from the set $\{1, 2, 3, 4\}$. Indeed, the Kronecker product $\mathbf{q} \otimes \mathbf{q}$ will result in a 16-dimensional vector containing 6 extra cross terms that are contained in the ten multisets.

As a direct consequence of this redundancy for a representation of $2n$ multivariate polynomials of degree i in the variables \mathbf{q} , there will be infinitely many possible representations for the nonlinear coefficient matrix \mathbf{G}_i corresponding to the i^{th} order in equation (5). We show this in Example 3.

Example 3. [*Multiple representations for the matrices \mathbf{G}_i*] If we assume, for simplicity, that $\mathbf{q} = (q_1, q_2)^T \in \mathbb{C}^2$, and $\mathbf{G}(\mathbf{q})$ is only of $\mathcal{O}(|\mathbf{q}|^2)$, i.e. $\Gamma = 2$,

$$\begin{aligned} \mathbf{G}(\mathbf{q}) &= \sum_{i=2}^2 \mathbf{G}_i \mathbf{q}^{\otimes i} = \mathbf{G}_2 \mathbf{q} \otimes \mathbf{q} = \begin{bmatrix} g_{11} & g_{12} & g_{13} & g_{14} \\ g_{21} & g_{22} & g_{23} & g_{24} \end{bmatrix} \begin{bmatrix} q_1^2 \\ q_1 q_2 \\ q_2 q_1 \\ q_2^2 \end{bmatrix} \\ &= \begin{bmatrix} g_{11} q_1^2 + (g_{12} + g_{13}) q_1 q_2 + g_{14} q_2^2 \\ g_{21} q_1^2 + (g_{22} + g_{23}) q_1 q_2 + g_{24} q_2^2 \end{bmatrix}. \end{aligned} \quad (\text{C.3})$$

Assume that the quadratic nonlinearities of the underlying system are modeled as follows

$$\mathbf{P}(\mathbf{q}) = \begin{bmatrix} a_1 q_1^2 + b_1 q_1 q_2 + c_1 q_2^2 \\ a_2 q_1^2 + b_2 q_1 q_2 + c_2 q_2^2 \end{bmatrix}. \quad (\text{C.4})$$

If we want to transform $\mathbf{P}(\mathbf{q})$ into the form of $\mathbf{G}(\mathbf{q})$, equating $\mathbf{G}(\mathbf{q})$ and $\mathbf{P}(\mathbf{q})$ and collecting terms of equal power in q_1 and q_2 gives

$$\begin{aligned} g_{11} &= a_1, & (g_{12} + g_{13}) &= b_1, & g_{14} &= c_1, \\ g_{21} &= a_2, & (g_{22} + g_{23}) &= b_2, & g_{24} &= c_2. \end{aligned}$$

The presence of the redundant term $q_2 q_1$ in $\mathbf{q} \otimes \mathbf{q}$ introduces two extra coefficients g_{13} and g_{23} , giving us the freedom to introduce a constraint between g_{12} and g_{13} , and between g_{22} and g_{23} . We then have two independent equations, each containing two independent variables. For each equation, an independent constraint can be introduced such that g_{12} , g_{13} , g_{22} and g_{23} are uniquely determined and the product $\mathbf{G}_2 \mathbf{q} \otimes \mathbf{q} = \mathbf{G}(\mathbf{q})$ precisely represents $\mathbf{P}(\mathbf{q})$. Each monomial term in the vector $\mathbf{q}^{\otimes i}$ has a unique location in the vector itself, which in turn points to a unique location in the matrix \mathbf{G}_i for each row. In this way, the constraints are automatically satisfied when SSMtool identifies the nonlinearities of the underlying mechanical system.

Appendix D. Memory requirements for the coefficient matrices

In our current setting, the most computationally demanding terms in the SSM construction are the summation terms in equation (31), which are shown below for the i^{th} order

$$\sum_{m=2}^{i-1} \mathbf{W}_m \sum_{|\mathbf{p}|=1} \mathbf{R}_{i+1-m}^{p_1} \otimes \dots \otimes \mathbf{R}_{i+1-m}^{p_m}, \quad (\text{D.1})$$

$$\sum_{m=2}^{i-1} \mathbf{G}_m \sum_{|\mathbf{r}|=i} \mathbf{W}_{r_1} \otimes \dots \otimes \mathbf{W}_{r_m}. \quad (\text{D.2})$$

If we assume that all matrices in equations (D.1) and (D.2) are densely filled with doubles, where each double has an allocated memory of 8 bytes in MATLAB, the total amount of memory needed (in bytes) to store the matrices in equations (D.1) and (D.2) corresponding to a mechanical system of n degrees of freedom at the i^{th} order is equal to

$$M(n, i) = 8 \cdot \sum_{m=2}^{i-1} ((2n)2^m + 2^{m+i}m + (2n)^{m+1} + (2n)^m 2^i c(m, i)), \quad (\text{D.3})$$

where $c(m, i)$ is the number of all possible combinations of m positive integers $l_1, \dots, l_m \in \mathbb{N}^+$, with $|\mathbf{l}| = i$.

Example 4. [*Memory requirements for different orders*] We consider a mechanical system of two degrees of freedom ($n = 2$) with a single cubic nonlinearity and arbitrary near-inner-resonances. The cubic nonlinear spring will only contribute to the \mathbf{G}_3 coefficient matrix, therefore the only contribution from equation (D.2) to equation (D.3) is for $m = 3$. In figure D.16, we show the output of equation (D.3) for different orders of expansion.

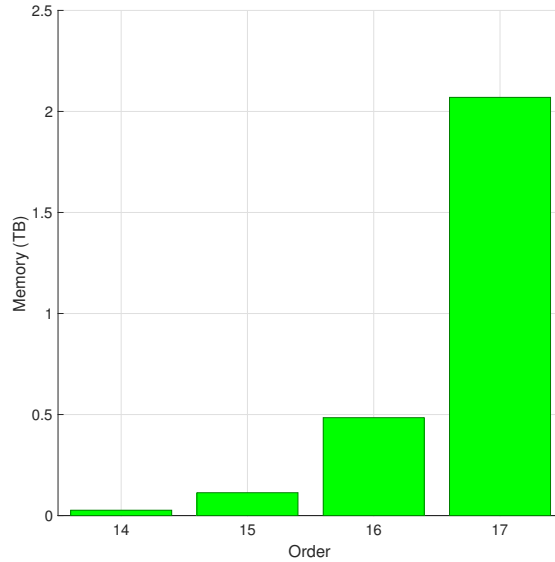


Figure D.16: Memory requirements in terabytes for equations (D.1) and (D.2) for different orders of the two-degree-of-freedom mechanical system. The amount of memory needed drastically increases from 0.4846 TB for order 16 to 2.0696 TB for order 17.

References

References

- [1] R. Rosenberg, The normal modes of nonlinear n-degree-of-freedom systems, *J. Appl. Mech.* 29 (1) (1962) 7–14. doi:10.1115/1.3636501.
- [2] S. Shaw, C. Pierre, Normal modes for non-linear vibratory systems, *J. Sound Vib.* 164 (1) (1993) 85–124. doi:10.1006/jsvi.1993.1198.
- [3] G. Kerschen, M. Peeters, J.-C. Golinval, A. Vakakis, Nonlinear normal modes, Part I: A useful framework for the structural dynamicist, *Mech. Syst. Sig. Process.* 23 (1) (2009) 170–194. doi:10.1016/j.ymsp.2008.04.002.
- [4] M. Peeters, R. Vigiú, G. Sérandour, G. Kerschen, J.-C. Golinval, Nonlinear normal modes, Part II: Toward a practical computation using numerical continuation techniques, *Mech. Syst. Sig. Process.* 23 (1) (2009) 195–216. doi:10.1016/j.ymsp.2008.04.003.
- [5] Y. Mikhlin, K. Avramov, Nonlinear normal modes for vibrating mechanical systems. Review of theoretical developments, *Appl. Mech. Rev.* 63 (6) (2010) 060802. doi:10.1115/1.4003825.
- [6] A. Vakakis, L. Manevitch, Y. Mikhlin, V. Pilipchuk, A. Zevin, Normal modes and localization in nonlinear systems, Springer, 2001. doi:10.1002/9783527617869.
- [7] A. Lyapunov, The general problem of the stability of motion, *Int. J. Control* 55 (3) (1992) 531–534. doi:10.1080/00207179208934253.
- [8] A. Kelley, Analytic two-dimensional subcenter manifolds for systems with an integral, *Pac. J. Math.* 29 (1969) 335–350. doi:10.2140/pjm.1969.29.335.
- [9] G. Haller, S. Ponsioen, Nonlinear normal modes and spectral submanifolds: existence, uniqueness and use in model reduction, *Nonlinear Dyn.* 86 (3) (2016) 1493–1534. doi:10.1007/s11071-016-2974-z.
- [10] R. Szalai, D. Ehrhardt, G. Haller, Nonlinear model identification and spectral submanifolds for multi-degree-of-freedom mechanical vibrations, in: *Proc. R. Soc. A*, Vol. 473, The Royal Society, 2017, p. 20160759. doi:10.1098/rspa.2016.0759.
- [11] G. Kerschen, K. Worden, A. Vakakis, J.-C. Golinval, Past, present and future of nonlinear system identification in structural dynamics, *Mech. Syst. Sig. Process.* 20 (3) (2006) 505–592. doi:10.1016/j.ymsp.2005.04.008.
- [12] M. Peeters, G. Kerschen, J.-C. Golinval, Dynamic testing of nonlinear vibrating structures using nonlinear normal modes, *J. Sound Vib.* 330 (3) (2011) 486–509. doi:10.1016/j.jsv.2010.08.028.
- [13] F. Blanc, C. Touzé, J. Mercier, K. Ege, A. Ben-Dhia, On the numerical computation of nonlinear normal modes for reduced-order modelling of conservative vibratory systems, *Mech. Syst. Sig. Process.* 36 (2) (2013) 520–539. doi:10.1016/j.ymsp.2012.10.016.
- [14] E. Pesheck, C. Pierre, S. Shaw, A new Galerkin-based approach for accurate non-linear normal modes through invariant manifolds, *J. Sound Vib.* 249 (5) (2002) 971–993. doi:10.1006/jsvi.2001.3914.
- [15] L. Renson, G. Delége, G. Kerschen, An effective finite-element-based method for the computation of nonlinear normal modes of nonconservative systems, *Meccanica* 49 (8) (2014) 1901–1916. doi:10.1007/s11012-014-9875-3.
- [16] X. Cabré, E. Fontich, R. De La Llave, The parameterization method for invariant manifolds I: manifolds associated to non-resonant subspaces, *Indiana Univ. Math. J.* 52 (2) (2003) 283–328. doi:10.1512/iumj.2003.52.2245.
- [17] X. Cabré, E. Fontich, R. De La Llave, The parameterization method for invariant manifolds II: regularity with respect to parameters, *Indiana Univ. Math. J.* 52 (2) (2003) 329–360. doi:10.1512/iumj.2003.52.2407.
- [18] X. Cabré, E. Fontich, R. De La Llave, The parameterization method for invariant manifolds III: overview and applications, *J. of Diff. Eq.* 218 (2) (2005) 444–515. doi:10.1016/j.jde.2004.12.003.
- [19] À. Haro, M. Canadell, J.-L. Figueras, A. Luque, J.-M. Mondelo, *The Parameterization Method for Invariant Manifolds*, Springer, 2016. doi:10.1007/978-3-319-29662-3.
- [20] J. van den Berg, J. Mireles James, Parameterization of Slow-Stable Manifolds and their Invariant Vector Bundles: Theory and Numerical Implementation, *Discrete Contin. Dyn. Syst* 36 (9). doi:10.3934/dcds.2016002.
- [21] J. Mireles James, Polynomial approximation of one parameter families of (un) stable manifolds with rigorous computer assisted error bounds, *Indagationes Mathematicae* 26 (1) (2015) 225–265. doi:10.1016/j.indag.2014.10.002.
- [22] A. Laub, *Matrix analysis for scientists and engineers*, SIAM, Philadelphia, 2005. doi:10.1137/1.9780898717907.
- [23] M. Géradin, D. Rixen, *Mechanical vibrations: theory and application to structural dynamics*, John Wiley & Sons, 2014.
- [24] S. Shaw, C. Pierre, Normal modes of vibration for non-linear continuous systems, *J. Sound Vib.* doi:10.1006/jsvi.1994.1021.
- [25] H. Dankowicz, F. Schilder, *Recipes for continuation*, SIAM, 2013. doi:10.1137/1.9781611972573.
- [26] G. Cirillo, A. Mauroy, L. Renson, G. Kerschen, R. Sepulchre, A spectral characterization of nonlinear normal modes, *J. Sound Vib.* 377 (2016) 284–301. doi:10.1016/j.jsv.2016.05.016.
- [27] J. Reddy, P. Mahaffey, Generalized beam theories accounting for von Kármán nonlinear strains with application to buckling, *J. of Coupl. Sys. and Mult. Dyn.* 1 (1) (2013) 120–134. doi:10.1166/jcsmd.2013.1006.
- [28] W. Lai, D. Rubin, E. Krempl, *Introduction to continuum mechanics*, Butterworth-Heinemann, 2009.
- [29] J. Skrzypek, A. Ganczarski, Constitutive equations for isotropic and anisotropic linear viscoelastic materials, in: *Mechanics of Anisotropic Materials*, Springer, 2015, pp. 57–85. doi:10.1007/978-3-319-17160-9_2.
- [30] G. Lesieutre, J. Kauffman, 'Geometric' Viscous Damping Model for Nearly Constant Beam Modal Damping, *AIAA J.* 51 (7) (2013) 1688–1694. doi:10.2514/1.j052174.
- [31] G. Lesieutre, Frequency-independent modal damping for flexural structures via a viscous "Geometric" damping model, *J. of guid., cont., and dyn.* 33 (6) (2010) 1931–1935. doi:10.2514/1.49864.

- [32] G. Takács, Basics of Vibration Dynamics, in: Model Predictive Vibration Control, Springer, 2012, pp. 25–64. doi: 10.1007/978-1-4471-2333-0_2.
- [33] J. Reddy, An Introduction to Nonlinear Finite Element Analysis: with applications to heat transfer, fluid mechanics, and solid mechanics, OUP Oxford, 2014.
- [34] R. Stanley, Enumerative Combinatorics. Vol. 1, vol. 49 of Cambridge Studies in Advanced Mathematics, Cambridge University Press, Cambridge, 1997.